





Article

# Road Runoff Characterization: Ecotoxicological Assessment Combined with (Non-)Target Screenings of Micropollutants for the Identification of Relevant Toxicants in the Dissolved Phase

Fidji Sandré <sup>1</sup>, Nina Huynh <sup>1</sup>, Marie-Christine Gromaire <sup>2</sup> , Gilles Varrault <sup>1</sup>, Christophe Morin <sup>1</sup> , Régis Moilleron <sup>1</sup> , Julien Le Roux <sup>1</sup>  and Laure Garrigue-Antar <sup>1,\*</sup> 

<sup>1</sup> Leesu, Ecole des Ponts, Université Paris Est Creteil, F-94010 Creteil, France; fidji.sandre@u-pec.fr (F.S.); tinh-nghi-nina.huynh@u-pec.fr (N.H.); varrault@u-pec.fr (G.V.); ch.morin@u-pec.fr (C.M.); moilleron@u-pec.fr (R.M.); julien.le-roux@u-pec.fr (J.L.R.)

<sup>2</sup> Leesu, Ecole des Ponts, Université Paris Est Creteil, F-77455 Marne-la-Vallée, France; marie-christine.gromaire@enpc.fr

\* Correspondence: laure.garrigue-antar@u-pec.fr



**Citation:** Sandré, F.; Huynh, N.; Gromaire, M.-C.; Varrault, G.; Morin, C.; Moilleron, R.; Le Roux, J.; Garrigue-Antar, L. Road Runoff Characterization: Ecotoxicological Assessment Combined with (Non-)Target Screenings of Micropollutants for the Identification of Relevant Toxicants in the Dissolved Phase. *Water* **2022**, *14*, 511. <https://doi.org/10.3390/w14040511>

Academic Editor: Rupak Aryal

Received: 27 December 2021

Accepted: 4 February 2022

Published: 9 February 2022

**Publisher's Note:** MDPI stays neutral with regard to jurisdictional claims in published maps and institutional affiliations.



**Copyright:** © 2022 by the authors. Licensee MDPI, Basel, Switzerland. This article is an open access article distributed under the terms and conditions of the Creative Commons Attribution (CC BY) license (<https://creativecommons.org/licenses/by/4.0/>).

**Abstract:** Road runoff (RR) is an important vector of micropollutants towards groundwater and soils, threatening the environment and ecosystems. Through combined chemical and biological approaches, the purpose of this study was to get insights on specific toxicants present in RR from two sites differing by their traffic intensity and their toxicological risk assessment. Non-target screening was performed by HRMS on RR dissolved phase. Ecotoxicological risk was evaluated in a zebrafish embryos model and on rat liver mitochondrial respiratory chain. Specific HRMS fingerprints were obtained for each site, reflecting their respective traffic intensities. Several micropollutants, including 1,3-diphenylguanidine (DPG) and benzotriazole (BZT) were identified in greater concentrations at the high-traffic site. The origin of DPG was confirmed by analyzing HRMS fingerprints from shredded tires. RR samples from each site, DPG and BZT were of relatively low toxicity (no mortality) to zebrafish embryos, but all generated distinct and marked stress responses in the light–dark transition test, while DPG/BZT mixes abolished this effect. The moderate-traffic RR and DPG inhibited mitochondrial complex I. Our study highlights (i) the unpredictability of pollutants cocktail effect and (ii) the importance of a multi-approaches strategy to characterize environmental matrices, essential for their management at the source and optimization of depollution devices.

**Keywords:** road runoff; micropollutants; HRMS; non-target screening; ecotoxicity; stress; light–dark transition; mitochondria; zebrafish

## 1. Introduction

Growing urbanization, increasing demographic pressure, and soil sealing generate important environmental pollution problems. Urban pollution originates from many sources, both endogenous and atmospheric to a lesser extent [1–6]. Part of this pollution is deposited on urban surfaces like roads and parking lots, which become major vectors of micropollutants towards groundwater and soils after rain events. Road runoff (RR) is constituted of a complex matrix of over 600 different micropollutants mainly originating from traffic, whose release can contribute to environmental degradation and cause a threat to aquatic organisms [7]. These pollutants include particles such as tire residues and dust, and molecules such as petrochemicals, metals, but also polycyclic aromatic hydrocarbons (PAHs), herbicides, phthalates, or alkylphenols [1,3,8,9].

Target analysis is one of the major tools to characterize wastewater and RR, allowing the detection and quantification of contaminants in the ng/L range [1,9–11]. Nevertheless, studies relying on target analysis do not detect nor evaluate pollutants on which no information exist, such as emerging contaminants, transformation products, and metabolites,

or which have not been searched specifically [12]. Thus, non-target screening (NTS) is increasingly used to complete the characterization of micropollutant contamination of samples without focusing on one or more families of molecules, but by examining the sample content as a whole, unraveling several hundreds to thousands of unknown molecules [13]. Few studies of this type have been carried out so far on RR samples [14,15] and even less coupling HRMS and toxicological analysis [16].

However, the only information on the presence of contaminants does not provide an assessment of the impact or the toxic potential of RR. Indeed, these micropollutants can not only have acute lethal effects on a wide range of species, but also negatively impact locomotor activities, feeding and reproduction individuals, populations, and ecosystems, at sub-lethal concentrations [17]. Thus, RR dissolved phase toxicity assessment is important not only for aquatic organisms as it is the main route of exposure, but also because of the possible infiltration in groundwater and potential impact on soil biodiversity. Furthermore, studies have shown that dissolved organic carbon (DOC), as well as other water parameters (alkalinity, hardness), can also modulate toxicity [18]. Therefore, it is necessary to evaluate the toxic potential by using appropriate integrative tests, sensitive enough to be responsive to environmental concentrations of individual substances close to- or even below the Environmental Quality Standard (EQS) or the detection limits, to provide an insight on the global toxic potential [19]. However, due to RR's extreme chemical complexity and cocktail(s) effects, establishing relationships between toxicants and biological effects, to date poorly understood, constitutes a major challenge for analytical chemists and ecotoxicologists [20–23].

Over the last two decades, zebrafish has become an increasingly popular vertebrate model for developmental studies, in vivo drug screening and environmental toxicity assessment [24,25]. Indeed, the zebrafish embryo is transparent small, and eggs can be obtained in great numbers, thanks to high fecundity. The zebrafish genome, with over 70% homology to human genes [26], is a relevant model for many human diseases and physiological processes [27–30]. Furthermore, its development is achieved within a few days, which makes this model more convenient and cost-effective than mammals to address systemic toxicity, teratological effects, and behavior [31–34]. Fish embryos are highly relevant to aquatic toxicity testing and have been long used in studies assessing single chemicals on which regulation programs such as the legislation REACH (Registration, Evaluation, Authorization, and Restriction of Chemicals) are based. Mixes of pollutants are now increasingly studied, in particular in urban runoff. Recently, coho salmon embryos and zebrafish larvae exposure to runoff pollutants was shown to generate long-lasting sublethal effects such as an alteration of the lateral line [35] or cardiotoxicity [36], related to the presence of PAHs. Another study showed that highway samples significantly increased mortality and the number of zebrafish embryos exhibiting anomalies, presumably by a synergistic effect between metals and PAHs [37]. Other works based on reconstituted mixtures—therefore less complex than those from the environment—proved to be an interesting approach for mechanistic studies but are less than satisfactory to interpret all the interactions between the different compounds [38–40]. Besides studies of functional and structural defects, behavioral approaches are environmentally relevant approaches to study the impacts of the pollutants on organisms, as behavior reflects many physiological processes, including neurodevelopment, metabolism, sensory organs, morphology, or molecular pathways alteration [33], and better indicates impacts on survival than measures of mortality. Indeed, several studies reported behavioral toxicity at concentrations 10 to 100 times lower than lethal concentrations [17]. A sensitive and reproducible behavior-based assay is the light–dark response test, as it measures stress through locomotor activity, which has been shown to provoke effects from exposures to compounds with or without known neuroactive properties [41,42].

In this study realized in the framework of the ROULÉPUR research program, we applied an original approach combining targeted/non-targeted screening and ecotoxicology to characterize RR micropollutants in the dissolved phase and their toxicological impact on the aquatic environment. NTS was performed using high-resolution mass spectrometry

(HRMS), and ecotoxicological assessment was done in a zebrafish larva model. Two sampling sites in the Paris metropolitan area were selected based on their difference in traffic intensity, one heavily trafficked suburban road [43,44], and the other with light to moderate urban traffic.

## 2. Materials and Methods

### 2.1. Study Sites and Sampling

Runoff was collected from two urban roads with contrasted traffic levels and traffic conditions and located in the Paris region: a  $2 \times 2$  lanes departmental road in a suburban area (Compans, C site) with high and smooth traffic (90 km/h speed,  $2 \times 11,000$  vehicles/day and a large proportion of heavy goods vehicles), and a  $2 \times 1$  lane street in a Town center (Rosny-sous-Bois, R site) with low and variable traffic (50 km/h speed, <3000 vehicles/day). The C site is located near an industrial zone including several SEVESO classified establishments and the Charles de Gaulle Airport.

In the framework of the ROULÉPUR project, samples were collected at these sites (along with two other sites) for an extended screening of traffic area runoff micropollutants. Runoff was collected from a storm drain (R site) or from a gully (C site). Details about the sampling methodology as well as extended results of target screening of micropollutants are provided in [9], published in the same special issue. In this work, only a fraction of samples from both sites were analyzed with HRMS or (eco)toxicological approaches, due to limited available volumes at the time of the experiments. Five samples collected at the C site in 2016 and 2017 (2016-05-30; 2016-06-14; 2017-01-09; 2017-03-01; 2017-04-30) and one at the R site (2018-03-29) were available for HRMS experiments. Three samples from the C site (2017-04-30; 2017-06-27; 2017-06-28) and one from the R site (2017-09-14) were available for (eco)toxicological analysis.

Additional experiments were conducted to obtain HRMS fingerprints of shredded tires and the related organic compounds that could potentially be released in water. Three types of shredded tires were selected for leaching tests and HRMS analyses (see Section 2.3) to compare the resulting chromatographic fingerprints with those from the study sites and to identify possible common peaks.

### 2.2. Global Parameters, 3D Fluorescence, and Targeted Screening

RR samples were analyzed for global parameters, including pH, electrical conductivity, total suspended solids (TSS), dissolved organic carbon (DOC) as previously described [43].

Dissolved organic matter (DOM) was characterized by 3D fluorescence. EEMs (fluorescence excitation/emission matrix) were obtained using a spectrofluorometer (FP-8300, 150-W Xenon lamp, Jasco) with the scanning range from excitation wavelength 240 nm to 450 nm at an interval of 5 nm and emission wavelength from 250 nm to 600 nm at an interval of 2 nm. If the UV254 was higher than  $0.050 \text{ cm}^{-1}$ , the samples were diluted with ultrapure water to avoid inner filter effects due to adsorbing species present in the wastewater [45]. EEMs of ultrapure water were subtracted from the sample EEMs and normalized by the Raman peak of ultrapure water at an excitation wavelength of 350 nm to obtain fluorescence data in Raman units (R.U.), and fluorescence intensities were corrected with dilution factors when needed [46]. Fluorescence peaks ( $\alpha$ ,  $\alpha'$ , and  $\beta$  peaks related to humic-like components,  $\gamma$  and  $\delta$  peaks related to protein-like components) were obtained at specific pairs of Ex/Em (excitation/emission) wavelengths from measured EEMs [47]. DOM quality was further evaluated by determining fluorescence ratios between peaks ( $\alpha'/\alpha$ ,  $\beta/\alpha$ ,  $\gamma/\alpha$ ,  $\delta/\alpha$ ) and two fluorescence indices—the humification index (HIX) [48] and the biological index (BIX) characteristic of recent autochthonous biological activity in water samples [49].

Targeted screening involved the analysis of 128 pollutants, including 41 inorganic and 87 organic pollutants or groups of substances, and is fully described in [9].

### 2.3. Non-Target Screening with HRMS

All runoff samples were processed and extracted within 48 h after collection. Samples were filtered on 0.7 µm glass fiber filters (GF/F, Whatman) and acidified to pH 2 with H<sub>2</sub>SO<sub>4</sub>. Prior to extraction, a mix of internal standards (bisphenol A-d6, propylparaben-d4, 4-n-octylphenol-d17 and 4-octylphenol-diethoxylate) was spiked in the samples at 200 ng/L. Extraction was carried out on Oasis HLB cartridges (Waters, Milford, MA, USA), conditioned successively with 5 mL dichloromethane, 10 mL ethyl acetate, 10 mL methanol, and 10 mL Milli-Q water acidified. 1 L of sample at pH 2 was loaded onto the cartridge, followed by 30 min drying with a gentle stream of N<sub>2</sub>. Elution was done with 3 mL dichloromethane, 5 mL ethyl acetate, and 5 mL methanol, and the extracts were stored at −18 °C prior to analysis. All extracts were analyzed in a single analytical sequence. Before analysis, extracts were concentrated with a stream of N<sub>2</sub> and reconstituted with 1 mL methanol/Milli-Q water (20/80 v/v) and filtered through a 0.2 µm PTFE filter.

The three selected types of shredded tires were extracted following two different protocols adapted from [50], a direct solvent extraction and a leaching followed by solid-phase extraction. In the first protocol, approximately 500 mg of tire particles were weighed and introduced into amber vials. 10 mL of methanol was added with 2 g of NaCl to facilitate extraction, and the mixture was shaken vigorously for 15 min. The supernatant was collected, filtered through a 0.2 µm PTFE syringe filter and evaporated to dryness under nitrogen flow. After recovery in 1 mL of ultrapure water/methanol mixture (80/20 v/v), the same mix of internal standards as the one used for runoff samples was added to the extract. In the leaching protocol, approximately 2.5 g of particulate matter was weighed and placed in amber vials. 500 mL of Volvic water diluted 21 times to simulate the mineralization of rainwater [51] were added and the mixture was agitated for 24 h. The sample was then filtered (GF/F, Whatman), acidified (pH 2 with sulfuric acid) and extracted following the same protocol than for runoff samples.

The extracts were analyzed with an ion-mobility time of flight mass spectrometry (IMS-QToF—Vion, Waters), equipped with an electrospray ionization source operating in positive (ESI+) and negative (ESI−) modes. Separation was performed with ultra-performance liquid chromatography (UPLC) using an Acquity BEH C18 column (1.7 µm, 2.1 mm × 100 mm, Waters, Milford, MA, USA) with its corresponding pre-column; 10 µL of each sample were injected at a rate of 0.45 mL/min with a mobile phase constituted of (A) Milli-Q water + 0.1% formic acid and (B) acetonitrile + 0.1% formic acid. The gradient was 1 min isocratic with 98% A, a 25 min linear decrease to 2% A, 5 min isocratic with 2% A, and a 4 min equilibration time with 98% A. ToF-MS analysis were carried out in data independent acquisition between 100 and 1000 Da. Samples were injected in randomized triplicates to minimize the intra-sequence variability caused by the instrument. Injection of blank samples (mobile phase) along with a pool sample (a mix of an equal volume of each sample injected during the sequence) every ten samples' injection was also used to evaluate the analytical drift. The good clustering of blank samples, pool injections as well as triplicate injections was verified by principal component analysis. More details about the quality check procedures are available elsewhere [52]. Data were acquired and pre-treated with UNIFI software (version 1.9.4.053, Waters) [53]. All detected features (i.e., triplets of m/z ratio, retention time and ion mobility drift time or collision cross-section (CCS) values) were aligned across the samples and exported as a csv file for further processing (i.e., visualization of HRMS fingerprints and statistical analyses) in the R software (version 4.1.2) [54]. Principal component analysis was performed on a total of 156,467 exported features with the *Morpho* [55] and *factoextra* [56] packages, and HRMS fingerprints were visualized using the *plotly* package [57].

Suspect screening was performed on the same data set, using a homemade library created in UNIFI software. Each suspect entry in the library contained the name of the molecule, its exact mass, its raw formula, and its structure, allowing *in silico* fragmentation. Suspects were targeted by their exact mass with a tolerance of 5 ppm and the detected fragments were compared to the predicted ones using a tolerance window of 2 mDa. When

a suspect was matched with sufficient evidence, its corresponding analytical standard was purchased for identity confirmation. Each acquired standard was prepared at three levels of concentration (500 µg/L, 50 µg/L, and 1 µg/L) and each level was injected five times using the defined analytical method. After the acquisition, the properties of the considered molecule (retention time, drift time, CCS, and fragments) were averaged between the injections and added to the library, along with information on the preferred ionization mode and detected adducts. This information is then used to confirm the suspect identity, using the previously described tolerance in mass, a tolerance of 0.2 min for retention time and a tolerance of 2% in CCS. Semi-quantitative comparisons were performed to compare the signals of some detected compounds between the samples. Normalized signals were obtained by dividing the intensity of a given compound by the intensity of an internal standard (propylparaben-d4) in the same sample and multiplying it by the intensity of the internal standard in the nearest pool sample.

## 2.4. Biological Approaches

### 2.4.1. Animals

Adult zebrafish (*Danio rerio*) were maintained and bred according to the National and European Guidelines for Animal Welfare at the University of Paris-Est Créteil. Tanks were maintained with a 14:10 h light:dark cycle with controlled conditions with a temperature between 26 and 28 °C, pH between 7.0 and 7.5, without chlorine. Males and females were kept in separate tanks until matching. We used the wild-type Tuebingen/AB fish line (ZFIN id: ZDB-GENO-010924-10) for all the experiments. Exposures were planned in accordance with the ethical rules in animal experimentation following the European Union (EU) Directive 2010/63/EU recommendations [58,59].

### 2.4.2. General Fish Breeding

For eggs collection, adult zebrafish were placed in a breeding tank with a female–male ratio of 2:1. Eggs were produced shortly after the lights were turned on and were collected promptly in a petri dish. The eggs were washed three times and maintained in standard E3 medium (146 mg/L NaCl; 6.3 mg/L KCl; 24.3 mg/L CaCl<sub>2</sub>; 40.7 mg/L MgSO<sub>4</sub>) at 26 °C. After 24 h, viable eggs were distributed in 96-well plates (1 egg per well) in E3 medium until exposure to RR samples or molecules.

### 2.4.3. Embryos Exposure

All experiments were carried out between the first day post-fertilization (dpf) and 139.5 h post-fertilization (hpf) (6 dpf: stage at which the larva is able to feed independently), as this is the limit for non-protected/non-regulated stages at 26 °C in the sense of EU Directive 2010/63/EU [59,60]. Chronic and acute exposures were carried out in parallel on the larvae of the same spawning. For chronic exposure, E3 medium was replaced by the 0.2 µm-filtered exposure solution, from 24 hpf until 6 dpf. The developmental staging was made according to [61]. For acute exposure, the E3 medium was replaced by 0.2 µm-filtered exposure solution for 24 h when zebrafish larvae reached 5 dpf. For each condition, 12 larvae were tested, and 3 replicates were made using different laying to limit genetic bias for a total of 36 larvae per solution for both chronic and acute exposure.

### 2.4.4. Teratology Screening and Behavioral Testing

Zebrafish larvae were screened for gross developmental abnormalities using a binocular magnifier. Different parameters were considered, such as the curvature of the body axis, cardiac defects, the presence of pericardial, yolk sac region edemas, structural malformation of the swimbladder, and mortality. Light–dark stress was then assessed at 5 and 6 dpf. The plates were placed into a Zebrabox (ViewPoint, Lyon, France) fitted with a camera that recorded larvae activity. The light–dark transition stress test was conducted following protocol by [41]. Briefly, the test begins with a 50 min acclimatization period for the larvae,



followed by three successive periods of 10 min of light and 5 min of darkness. The distance moved is quantified with the ZebraLab software (version 3.22.3.73).

#### 2.4.5. RR Samples and Chemicals Preparation

RR samples from the two sites were stored at  $-20\text{ }^{\circ}\text{C}$  in glass bottles until use. After thawing, they were filtered on a  $0.2\text{ }\mu\text{m}$  diameter cellulose acetate syringe filter (Macherey Nagel, Hoerdtt, France). Concentrated E3 medium was added to the exposure solutions in order to provide the necessary conditions for the development of the larvae in the area. 1,3-diphenylguanidine (DPG) and benzotriazole (BZT) were purchased from Sigma-Aldrich and prepared in E3 medium at the indicated concentrations.

#### 2.4.6. Assay of Mitochondrial NADH-Ubiquinone Reductase (Complex I) Activity

Isolation of rat liver mitochondria was performed as previously described [62]. Briefly, the liver was homogenized ( $6\text{ mL/g}$  of tissue) in ice-cold isolation buffer (Tris-HCl  $20\text{ mM}$ , sucrose  $250\text{ mM}$ , KCl  $40\text{ mM}$ , EGTA  $2\text{ mM}$ , and bovine serum albumin  $1\text{ mg/mL}$ , pH  $7.2$  at  $4\text{ }^{\circ}\text{C}$ ) using a Potter–Elvehjem homogenizer. Mitochondria isolation was immediately performed at  $4\text{ }^{\circ}\text{C}$  by differential centrifugation. The homogenate was centrifuged at  $2000\text{ g}$  for  $8\text{ min}$  to remove cell debris and nuclei. Mitochondria were recovered from the supernatant by centrifugation at  $12,000\times g$  for  $11\text{ min}$ . Mitochondria were washed and resuspended in a respiration buffer containing  $\text{KH}_2\text{PO}_4$   $10\text{ mM}$ , KCl  $10\text{ mM}$ ,  $\text{MgCl}_2$   $5\text{ mM}$ , pH  $7.2$  at  $37\text{ }^{\circ}\text{C}$ . The protein concentration of the mitochondrial suspension was determined by BCA assay.

The enzyme activity of complex I is measured indirectly through the activity of complex III which reduces cytochrome C. Cytochrome C absorbance at  $550\text{ nm}$  was quantified by a Jasco-730<sup>®</sup> double-beam spectrometer, at  $37\text{ }^{\circ}\text{C}$ . In both test-cell and reference cell,  $200\text{ }\mu\text{g}$  of mitochondria, KCN  $1\text{ mM}$ , cytochrome C  $10\text{ mM}$ , respiration buffer or test molecule at the given concentration were added to a quartz cell. Rotenone  $2\text{ }\mu\text{M}$ , a specific inhibitor of complex I, was added to the reference cell. After  $2\text{ min}$ , the reaction was started by injecting NADH  $6.3\text{ mM}$ .

### 3. Results

#### 3.1. Overview of the Two Sites: Global Characterization

The two study sites were chosen because of their contrasted situation in terms of traffic: a road with high traffic (C site) and an area with moderate traffic (R site). Detailed analyses of both sites at all sampling dates are provided in [9] (this issue) and summarized in Table 1 for samples selected in this work. Briefly, the C site is characterized by higher TSS concentrations, correlating with its high traffic, while these concentrations vary widely in the R site, with the highest concentrations possibly related to a building site nearby. Conductivity also showed some variability, mainly attributed to deicing salt applied at the C site (2017-01-09 and 2017-03-01), and illegal dumps of construction materials at the R site (2018-03-29). DOC concentrations, as well as pH ranges, were comparable between the two sites. The samples intended for HRMS and (eco)toxicity experiments were globally representative of their respective sites of origin (i.e., as compared to ranges of parameters measured over all sampling campaigns).

Further characterization of the samples by 3D fluorescence spectroscopy revealed a significant difference between the two sites in terms of quantity of the fluorescent organic matter. Apart from fluorophore  $\gamma$ , the fluorophores  $\alpha$ ,  $\alpha'$ ,  $\beta$ , and  $\delta$  showed significantly higher intensities at the C site (Figure S1). Even when normalizing the results by the dissolved organic carbon (DOC) values of the samples, fluorescence intensities were still significantly higher for most fluorophores ( $\alpha$ ,  $\alpha'$ ,  $\beta$ , and  $\delta$ ), which indicates that the samples from the C site contained a more important amount of fluorescing organic compounds than the ones from the R site. Fluorescence ratios between fluorophores ( $\alpha'/\alpha$ ,  $\beta/\alpha$ ,  $\gamma/\alpha$ ,  $\delta/\alpha$ ) as well as humification (HIX) and biological (BIX) indexes were calculated to get more qualitative information about DOM. The variability of these indexes was generally higher at

the C site, especially because three samples exhibited greater values for most fluorescence ratios and indexes. Those three samples were, however, not part of the samples used for HRMS and ecotoxicity assessment, which did not show significantly different results between the two sites. HIX values were small, indicating a low humification of the dissolved organic matter (DOM). Fluorescence excitation–emission matrices (EEMs) indicated that the two sites differ more by the molecules amounts present in the samples rather than the nature of these molecules. The samples selected for ecotoxicity assessment and HRMS analysis were also in the typical range of samples in terms of fluorescence intensity.

**Table 1.** Physico-chemical characteristics of runoff samples: median, (C10–C90) concentrations for all samples collected during the campaigns [9], with a focus on those characterized by HRMS and ecotoxicity (corresponding dates are indicated). TSS = total suspended solids; Cond. = conductivity; DOC = dissolved organic carbon; C = Compans site; R = Rosny site.

Site	Sampling Date	TSS (mg/L)	pH	Cond. (µS/cm)	DOC (mg C/L)
C	all samples	249.0 (99.8–597.4)	8.0 (7.6–8.4)	200.3 (93.2–1852.6)	5.9 (3.6–11.5)
	2016-05-30	71.7	8.0	87.9	1.7
	2016-06-14	172.2	8.0	156.7	6.2
	2017-01-09	582.3	8.4	1949.5	5.7
	2017-03-01	932.8	8.4	530.5	5.6
	2017-04-30	231.9	7.8	304	10.7
	2017-06-27	733.6	7.8	93.8	8.5
	2017-06-28	532.5	8.1	265.2	14.2
R	all samples	44.4 (17.3–442.8)	7.9 (7.6–9.4)	152.8 (113.9–450.4)	8.5 (4.7–16.8)
	2017-09-14	51	7.9	122.9	8.5
	2018-03-29	738	9.0	465.0	13.7

Targeted screening was performed on several families of micropollutants: metals, phthalates, alkylphenol ethoxylates and carboxylates, bisphenol A (BPA), polycyclic aromatic hydrocarbons (PAHs) (Table 2). Concentrations measured in the samples of the present study were within the typical concentration ranges obtained at the two sites [9]. As a whole, contamination profiles appeared quite similar between the two sites, which was unexpected given their respective traffic intensities. In specific cases (e.g., 4-nonylphenol, BPA), some median concentrations were even higher at the R site, but overall ranges were comparable.

### 3.2. (Eco)Toxicity Assessment of RR Samples on Zebrafish Larvae Development and Behaviour

#### 3.2.1. Toxicity of RR Samples

No significant gross abnormalities were observed during the 6 day-exposure of the larvae to the RR samples (chronic exposure) or during the exposure performed from 5 to 6 dpf (acute exposure) compared to controls. The only defects observed in both cases was a lack of control of buoyancy, resulting from a deflated swimbladder, or abnormal spine curvature but they did not reach statistical significance. Furthermore, the two RR samples did not produce any mortality. Thus, these tests did not appear sensitive enough to detect any toxicity in this time lapse.

#### 3.2.2. Light–Dark Stress Test

Behavioral studies may give some clues about pollutants' impacts on organisms. The light–dark transition test is appropriate as it induces stress evaluated by the distance moved by the larvae, a measurable parameter to assess toxic substances impacts [41,63]. Thus, locomotor activity following alternating light–dark photostimulation was analyzed for 6 dpf-old zebrafish larvae exposed to RR samples (Figure 1).

**Table 2.** Summary of targeted analyses of runoff samples (dissolved phase) from the C and R sites: median, min and max concentrations ( $\mu\text{g/L}$ ) measured for all samples collected at these sites ([43], doi:10.17632/m8kcmthfd2.1) and for samples used in this work. All analyses were not systematically performed from all samples (due to volume limitations) (NA = calculation not applicable). DEHP = di(2-ethylhexyl)phthalate; NP = 4-nonylphenol; OP = 4-*tert*-octylphenol; BPA = bisphenol A;  $\Sigma\text{PAHs}$  = sum of 16 polycyclic aromatic hydrocarbons; C = Compans site; R = Rosny site; ND = not detected (<limit of quantification).

Substances	Concentrations ( $\mu\text{g/L}$ )—Median (Min–Max)					
	C			R		
	All Campaigns	Samples for HRMS	Samples for Ecotoxicity	All Campaigns	Sample for HRMS	Sample for Ecotoxicity
Cu	26 (14–42)	27 (22–38)	30 (23–38)	11.1 (4.6–19.3)	4.6	NA
Zn	32 (16–71)	32 (22–66)	32 (22–43)	18.9 (2.4–53.5)	2.4	NA
Ni	1.1 (0.6–4.5)	1.3 (0.7–4.5)	1.1 (0.8–1.4)	1.5 (1.1–10.0)	10.0	NA
Pb	0.4 (0.2–0.9)	0.3 (0.2–0.5)	0.3 (0.2–0.4)	0.6 (0.3–1.4)	ND	NA
Ti	4 (2–76)	2 (2–76)	3 (ND–3)	28 (1–81)	4	NA
DEHP	3.4 (0.9–12.1)	2.5 (1.6–3.6)	3.6 (0.9–4.7)	1.2 (1.0–1.9)	1.9	ND
NP	386 (99–752)	307 (189–752)	386 (99–752)	477 (311–774)	578	376
OP	126 (33–224)	166 (117–194)	114 (72–166)	97 (32–223)	141	52
BPA	280 (66–696)	280 (225–499)	265 (225–609)	535 (306–716)	397	716
$\Sigma\text{PAHs}$	61 (40–212)	132 (60–212)	61 (50–68)	86 (29–115)	86	ND

In these conditions, in normal larvae, the rapid transition from light to dark generates stress, which results in a burst of swimming activity. When the light is turned back on, activity drops to the initial level and increases rapidly and sharply again when darkness returns [41,64]. This pattern was observed in all groups tested and the two conditions (6 day “chronic” exposure from 1 dpf, or 24 h “acute” exposure from 5 dpf). For larvae exposed to RR from the C site (Figure 1), no significant differences were seen between control and RR larvae during light periods in chronic exposure (panels A, B, C), while in acute exposure, larval activity was increased very significantly in two samples (2017-04-30 and 2017-06-27) or without reaching significance (2017-06-28). In contrast, during dark periods (panels D, E, F), the larvae exposed to RR samples (panels E, F) moved significantly less than the control larvae ( $p < 0.001$ ) in both conditions. Noteworthy, the 2017-04-30 sample (panel D) did not change the larval activity in both types of exposure.

A different profile of responses was observed for larvae exposed to RR from the R site (Figure 2), with no significant difference in the distance moved between control and exposed larvae in both conditions during the dark periods (panel B), while in the light period, the RR-exposed larvae were significantly hypoactive in chronic exposure ( $p < 0.001$ ), and hyperactive ( $p < 0.05$ ) compared to controls in acute exposure (panel A).

Taken together, these results show that despite the relatively apparent low toxicity regarding mortality and developmental abnormalities endpoints, exposure to the RR micropollutants from the R and C sites results in distinct stress response patterns affecting larvae behavior. For all these RR samples, behavioral toxicity is observed in chronic and acute conditions.

### 3.2.3. Mitochondrial Respiratory Chain Complex I

Mitochondrial dysfunction can result from environmental pollutants exposure (e.g., pesticides, herbicides, biocides, industrial and pharmaceutical compounds) even at low concentrations, which target the respiratory chain complexes and, in particular, the complex I (NADH-coenzyme Q oxidoreductase) [65,66]. Our results showed that the mitochondrial complex I activity is not impacted by a RR sample (2017-06-28) from the C site but is significantly inhibited by the R site one (41.25%) (Figure 3).



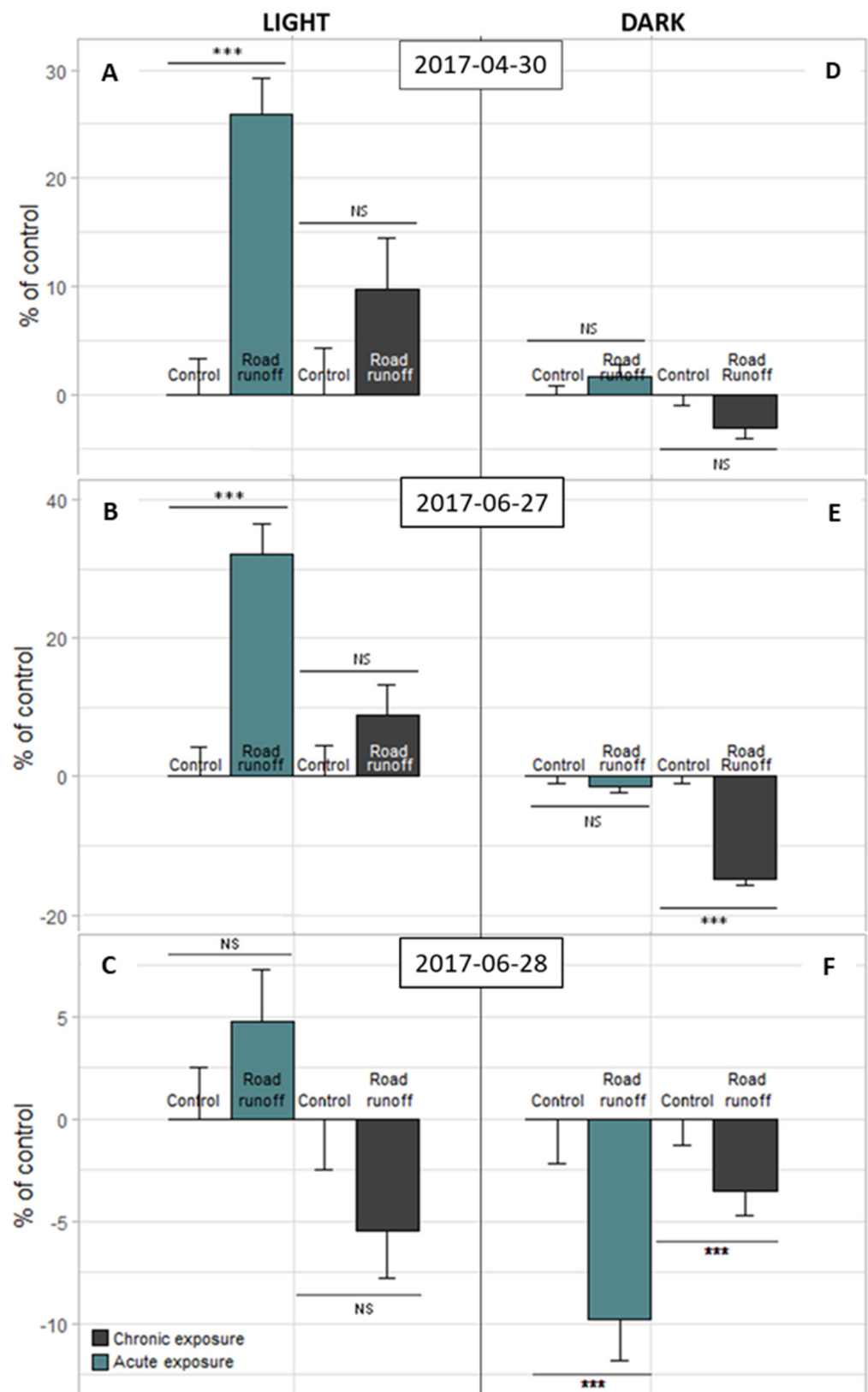


**Figure 1.** Activity (% of control) of 6 dpf old zebrafish larvae exposed to RR from C site in chronic and acute exposure (A–C): light condition; (D–F): dark condition. Control = E3 solution; number of larvae = 36 per condition; NS = not significant; \* =  $p$ -value < 0.05; \*\* =  $p$ -value < 0.01; \*\*\* =  $p$ -value < 0.001 (non-parametric Kruskal–Wallis test). Error bars represent the standard error.

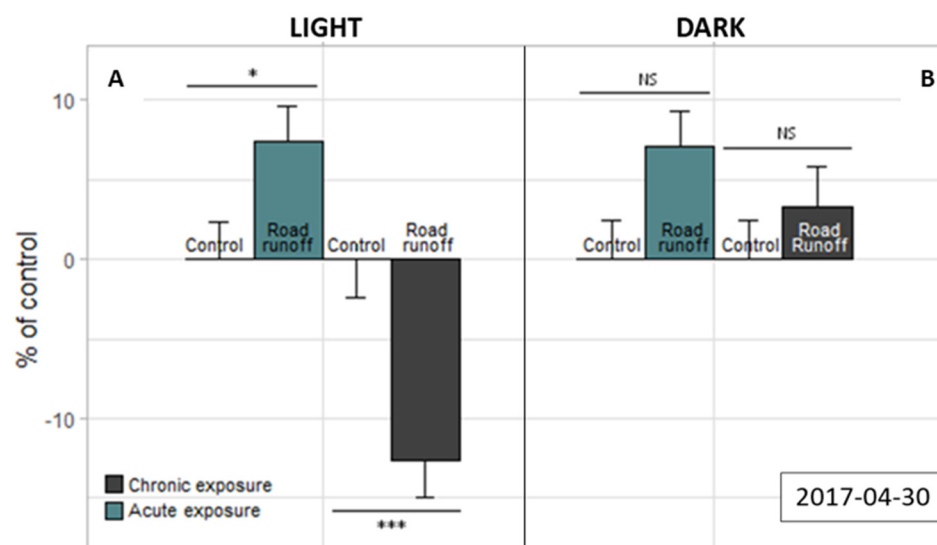


**Figure 2.** Activity (% of control) of 6 dpf old zebrafish larvae exposed to RR from R site in chronic and acute exposure. Light period (A); dark period (B). control = E3 solution; number of larvae = 36 per condition; NS = not significant; \* =  $p$ -value < 0.05; \*\* =  $p$ -value < 0.01; \*\*\* =  $p$ -value < 0.001 (non-parametric Kruskal–Wallis test). Error bars represent the standard error.

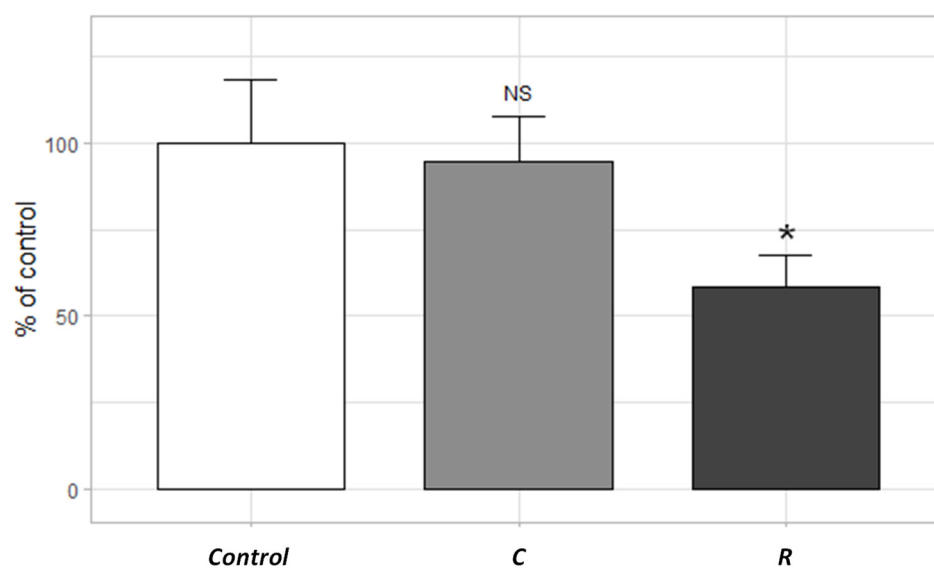


**Figure 3.** Inhibition of complex I of the mitochondrial respiratory chain induced by RR samples from the Compans (C) and Rosny (R) sites (2017-06-28 and 2017-09-14, respectively). Difference compared to control \* =  $p$ -value < 0.05 (non-parametric Kruskal–Wallis test); NS = not significant.

### 3.3. Non-Target Screening and Identification of Specific Micropollutants by HRMS

A principal component analysis was first performed using the table of features detected by HRMS from all samples to visualize the variability between the two sites and the various sampling times at the C site (Figure 4). For each sample, the three injection replicates were very close, demonstrating the instrumental stability. As already observed with results comprising even more samples and sites [9], the two sites were very well discriminated (along the first principal component PC1 representing 12.4% of the variance). The two sites indeed exhibited very distinct HRMS fingerprints, with more features and generally higher intensities in the C samples. Three samples from the C site exhibited similar HRMS profiles (2016-05-30, 2016-06-14, 2017-01-09) while one sample (2017-03-01) was very different and a last one (2017-04-30) showed an intermediate profile. These samples showed a high

temporal variability in terms of detected features and were thus discriminated along with the second principal component (8% of the variance). Despite the lower number and intensity of features detected at the R site, it exhibited a very specific HRMS fingerprint (Figure S2).

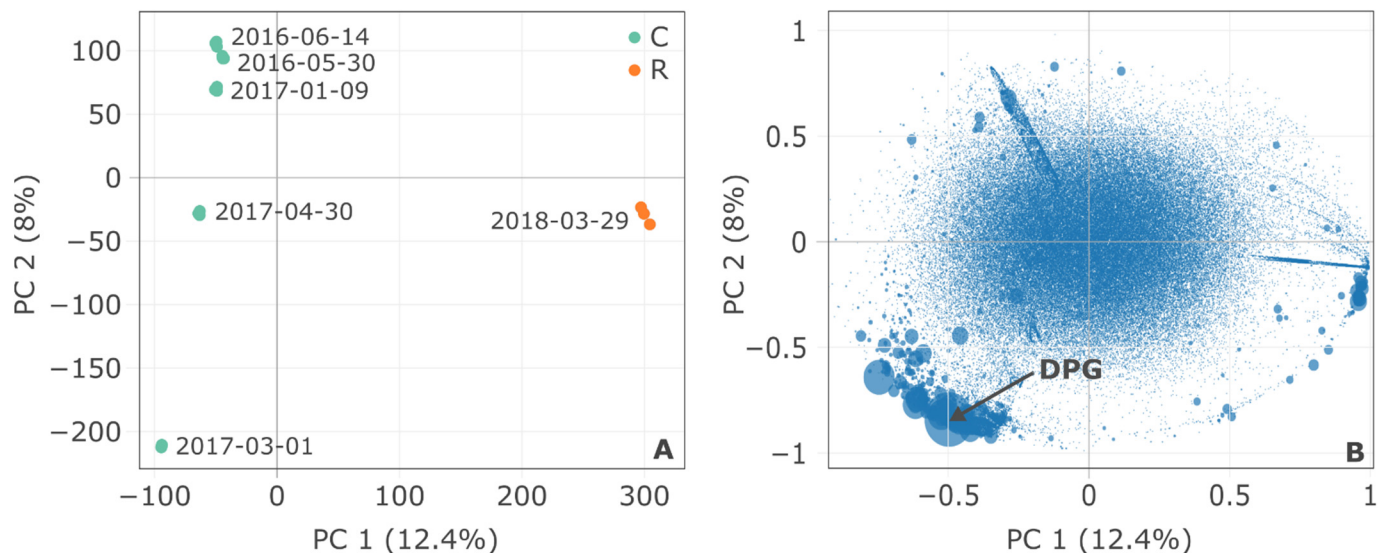


**Figure 4.** Principal component analysis of HRMS features. (A) Scores plot showing samples with corresponding sampling dates for the C and R sites; (B) Loadings plot showing all features detected in the samples, with the size of bubbles proportional to the highest intensity of a given feature among all samples.

By following a Kendrick mass defect (KMD) approach [67], some homologous series of compounds were detected at the R site, and at the C site sampled on 2017-03-01 (Figure 5). At the C site, several features showed a KMD of  $0.0248 \pm 0.0004$  and were all separated by 44.0263 mass units: features at  $m/z$  287.1458 and 331.1721; features at  $m/z$  349.1827, 393.2090 and 437.2353; and features at  $m/z$  481.26144, 525.2880, 569.3144, 613.3408, 657.3671, 701.3933, and 745.4198. These molecules exhibited a regular increase in their retention time and ion mobility drift time, confirming them as part of homologous series. The 44.0263 mass difference corresponds to an ethoxylated structure of  $(-\text{CH}_2-\text{CH}_2-\text{O}-)$  (exact mass of 44.0262), which could originate from polyethylene glycols (PEGs) or linear alkyl ethoxylates [68,69]. This series of molecules did not show fragment ions at higher collision energies, which often occurs with  $[\text{M}+\text{Na}]^+$  adducts. Taking sodium into account in the calculation of molecular formulas, they were identified by UNIFI as PEGs (e.g.,  $m/z$  393.2090 was identified as octaethylene glycol) (Table S1). Other series of homologous compounds were detected in the C site samples with a 44.0263 mass difference, with KMD values of  $-0.0228 \pm 0.0006$  (proposed formulas  $\text{C}_{2n+5}\text{H}_{4n+15}\text{N}_5\text{O}_n$ ), or with a 58.0418 mass difference. Raw formulas were calculated with good confidence and were consistent between molecules of each series, but no molecular structures were proposed or found in online databases (Table S1). Similar homologous series of compounds were found in the samples from the R site, with a 44.0263 mass difference. A first series was identified as PEGs monomethyl ethers, while others corresponded to a raw formula of  $\text{C}_{2n+4}\text{H}_{4n+8}\text{N}_4\text{O}_n$  and  $\text{C}_{2n+6}\text{H}_{4n+17}\text{N}_5\text{O}_n$  but were not proposed any molecular structure.

A peak presented a high intensity in the C samples and was observed in all samples at a retention time of 5.02 min, with an  $m/z$  of 212.1178 and a CCS value of  $143.5 \text{ \AA}^2$  (in ESI+ mode). It was the most intense peak in the 2017-03-01 sample from the C site (Figure 4) and was tentatively identified as 1,3-diphenylguanidine ( $\text{C}_{13}\text{H}_{13}\text{N}_3$ —DPG). DPG, as well as 1,3-di-o-tolylguanidine, are used as accelerators in the vulcanization processes of rubber and were identified and quantified at the ng/L level in surface water and groundwater samples

across Europe [70]. DPG was also reported at up to 300 µg/l in stormwater in Canada [71]. It was purchased as an analytical standard for unambiguous detection and its presence was confirmed in the samples. DPG intensities were extracted from all samples. DPG showed a high variability at the C site and exhibited a much lower intensity at the R site, in accordance with their respective traffic (Figure 6). Another feature at  $m/z$  277.1904 with a retention time of 6.89 min and a CCS value of 164.2 Å<sup>2</sup> was highly correlated with the occurrence of DPG among the samples, corresponding to a proposed formula of C<sub>14</sub>H<sub>26</sub>N<sub>2</sub>O<sub>2</sub> and tentatively identified as 4-[(2,2-dimethylpropanoyl)amino]-N,N-diethylbenzamide.

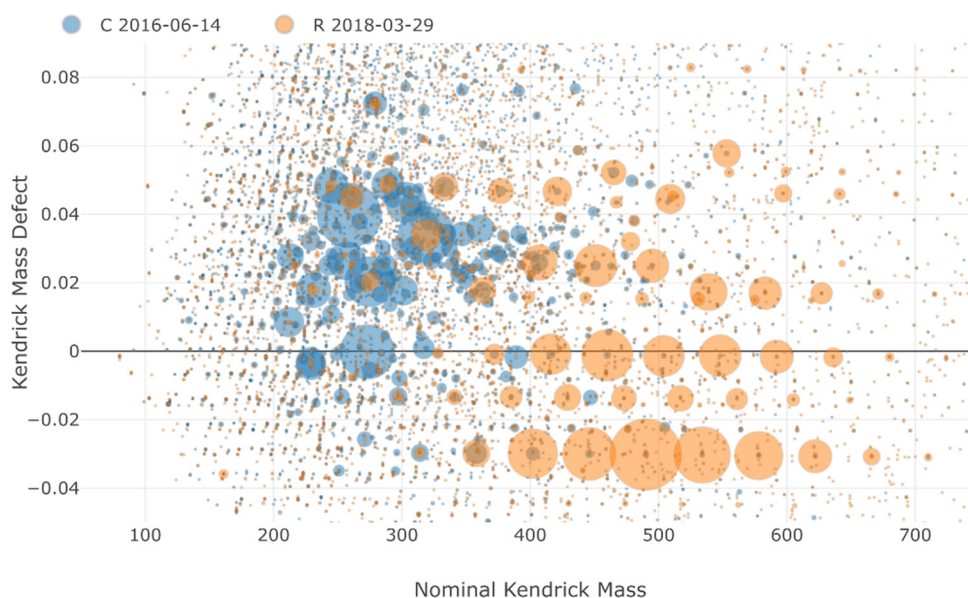


**Figure 5.** Kendrick mass defect plot for samples from C site (2016-06-14) and R site (2018-03-29), showing characteristic series of homologous compounds at the R site. The size of bubbles is proportional to the intensity of the features.

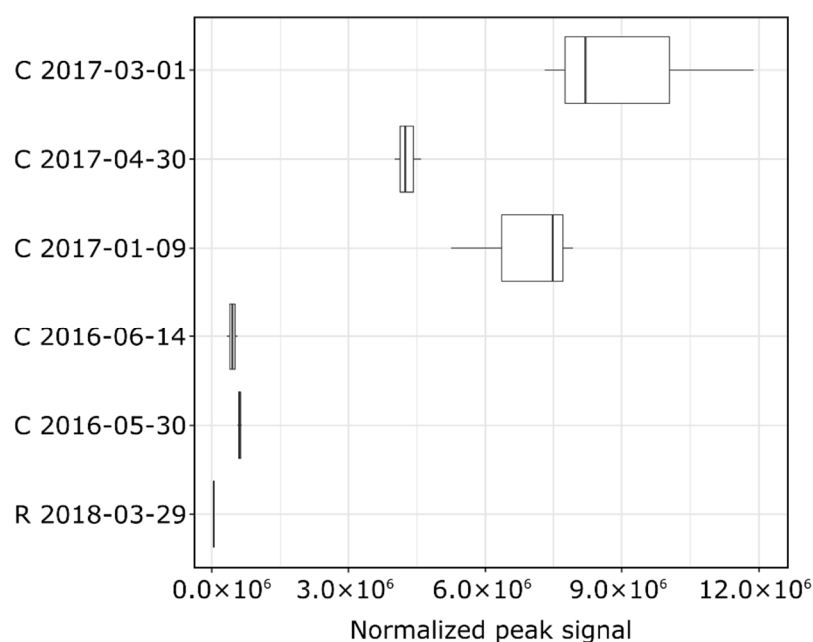


**Figure 6.** Boxplots representing the intensities of 1,3-diphenylguanidine in each sample (triplicate injections), normalized by the intensity of propylparaben-d4 injected as internal standard. C = Compans site; R = Rosny site.

In the ESI<sup>−</sup> mode, less features were detected in all samples, but one of the most intense features ( $m/z$  213.9642 at 4.36 min and a CCS value of 139.23 Å<sup>2</sup>) was identified as 1,3-benzothiazole-2-sulfonic acid (C<sub>7</sub>H<sub>5</sub>NO<sub>3</sub>S<sub>2</sub>), a transformation product of another vulcanization accelerator (2-mercaptobenzothiazole) that was recently identified in wastewater [69]. Following the identification of these compounds originating from the composition of tires, several other compounds that could occur in RR because of a release from tires or from vehicles were searched in the samples. 6PPD, a common tire rubber antioxidant, was recently discovered as the precursor of 6PPD-quinone, a product responsible for the high mortality of Pacific North-west coho salmon exposed to urban runoff [72]. Benzotriazole (BZT) is used as a corrosion inhibitor in dishwashing detergents, and as antifreeze or aircraft deicing agent. It has been identified as persistent and ubiquitous in the aquatic environment where it is found at a wide range of concentrations (10 ng/L in groundwater; 25 µg/L in wastewater [73]), but to date, little is known about its ecotoxicological impacts. 6PPD was not detected in the samples, but 6PPD-quinone and BZT were potentially present. BZT presence was further confirmed by the injection of an analytical standard. It followed the same intensity distribution as DPG and 1,3-benzothiazole-2-sulfonic acid among the samples (Figures S4 and S5), with an important presence at the C site (2017-03-01) and a very low intensity at the R site. Its presence at the C site could be related to the location of this sampling point in the vicinity of Paris Charles de Gaulle international airport, as well as to the emission from cars (because of its similar profile to the one of DPG). Several peaks detected in the C site samples matched with the exact mass of 6PPD-quinone, but its presence could not be confirmed unambiguously because no standard was injected to confirm its retention time and drift time values. Among other compounds listed as specific to RR signatures (N-butylbenzenesulfonamide, hexa(methoxy)methylmelamine, or dicyclohexylamine, [14]), only dicyclohexylamine was also detected in the samples (at the C site) and followed the same trends as DPG.

Complementary experiments were performed to get HRMS fingerprints of shredded tires and to confirm the release of DPG in controlled conditions. Tires from three manufacturers were shredded and two types of leachates (with either simulated rainwater or methanol) were obtained. All chromatograms exhibited an intense peak that was also confirmed as DPG. Intensities from the simulated rainwater leachates were similar to those in the methanol extract, thus showing that DPG can easily be released from tires during rain events. The three types of tires showed contrasted leaching of DPG, and the same trend was observed with both leaching methods. Overall, HRMS fingerprints from either type of leachates exhibited very similar features. Some homologous series of compounds were detected for two types of tires (Figure S6), but they were present in low intensities and were distinct from homologous features detected in RR samples. 6PPD was detected with high intensities in the methanol leachates and at much lower intensities in simulated rainwater leachates, even though one type of tire released important amounts of 6PPD when exposed to water. Other compounds were tentatively identified (Table S2) and some of them were also detected in RR samples (site C 2017-03-01). Most of them contained nitrogenous moieties and aromatic groups (e.g., 2-amino-N-cyclohexylbenzamide). More work would, however, be needed to definitely confirm the molecular structures of these compounds, and additional sampling of RR would be required to confirm the presence of these molecules in environmental samples.

### 3.4. (Eco)Toxicity of 1,3-Diphenylguanidine & Benzotriazole

#### 3.4.1. Light–Dark Stress Test

We chose two realistic concentrations for each of these compounds separately (DPG: 1000 and 3000 ng/L; BZT 50 and 350 ng/L) as well as in mixture and studied larval activity during a light–dark test at 6 dpf after chronic and acute exposure to the molecules as described above (Figure 7).



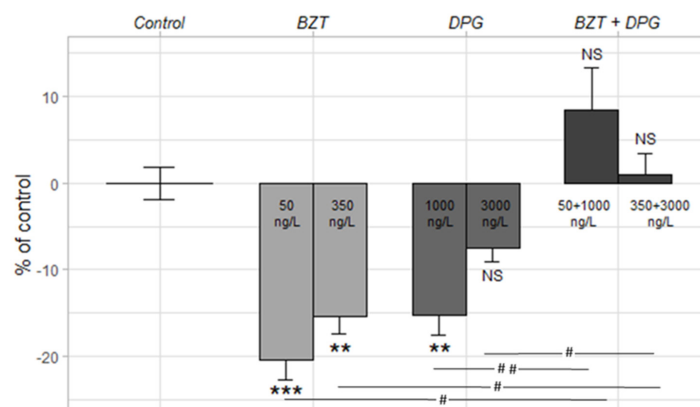


**Figure 7.** Activity (% of control) of 6 dpf old zebrafish larvae exposed to BZT and DPG in chronic exposure (dark period). Control = E3 solution, number of larvae = 12 per condition; NS = not significant; \*: difference compared to control. # =  $p$ -value < 0.05; \*\* =  $p$ -value < 0.01, \*\*\* =  $p$ -value < 0.001 (non-parametric Kruskal–Wallis test). Error bars represent the standard error.

No significant mortality nor deformities were observed in these two conditions. In acute exposure to BZT, DPG, or to the two mixes, no significant differences were observed at all concentrations tested in dark and light conditions compared to controls (data not shown).

In chronic exposure, BZT significantly inhibited larvae activity at 50 and 350 ng/L in dark periods, reaching 15 to 20% less distance moved compared to control, with no significant difference between the two concentrations. Similarly, DPG at 1000 ng/L inhibited the distance moved by the larvae by 15%, while the highest concentration, unexpectedly, failed to do so significantly. The difference between the effects of these two concentrations was not significant either. We also examined the effect of mixes (low and high concentration combinations) on larval activity. Unlike the single compounds, both high and low concentration mixtures had no inhibitory effect on larval activity compared to controls. However, the effects of both mixes effects were significantly different from those of the corresponding single-molecule concentrations.

### 3.4.2. Mitochondrial Respiratory Chain Complex I

Our results showed that the mitochondrial complex I is significantly inhibited by DPG at both concentrations by more than 50% compared to control, but without reaching statistical significance by BZT (Figure 8).

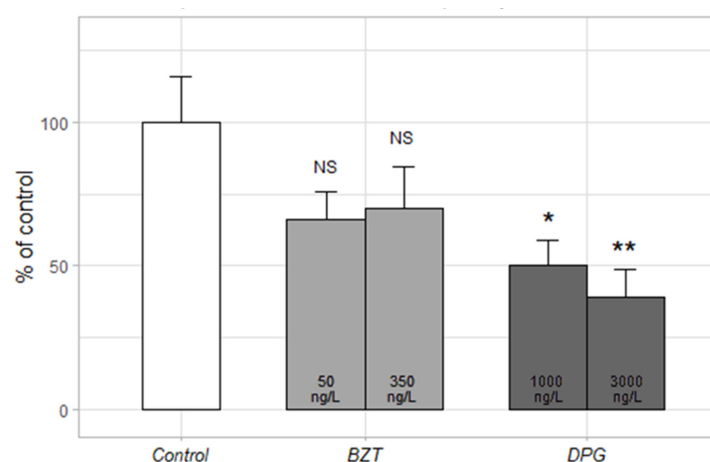


**Figure 8.** Inhibition of complex I of the mitochondrial respiratory chain by BZT and DPG at the indicated concentrations. Difference compared to control \* =  $p$ -value < 0.05, \*\* =  $p$ -value < 0.01 (non-parametric Kruskal–Wallis test); NS = not significant.

#### 4. Discussion

In the present study, we observed that despite their relatively apparent low toxicity regarding mortality and developmental abnormalities endpoints, exposure to the micropollutants from both sites resulted in distinct stress response patterns affecting larvae behavior, and with potentially adverse effects on survival at later time points in the larvae life. Indeed, both larvae' hypo- or hyperactivity makes them more vulnerable to predators, hypoactivity preventing them from escaping rapidly, and hyperactivity/stress resulting in exhaustion of their energy sources and loss of mobility [34]. This can also potentially impact their reproduction, as stressed fish may unnecessarily seek shelter resulting in reduced mating opportunities and ability to find food. In other studies, exposure of zebrafish larvae to various phthalates (DMP, DBP, di (2-ethylhexyl) phthalate (DEHP), DEP . . . ) [74,75], which were present at both sites [9], have been reported to induce alteration of locomotor activity, possibly through transcriptional alterations of the spinal developmental genes, or negative impacts on the central nervous system and the brain of the developing larvae. Furthermore, we showed that the use of the light–dark stress test at different stages of development provided additional relevant information on the impact of these samples. For all RR samples, behavioral toxicity was observed in chronic (exposure from the egg stage until 6 dpf) and acute (24 h exposure after the major developmental processes are established) conditions, underlining that these micropollutants have potentially multiple targets throughout the development and/or that the metabolizing enzymes are regulated differentially. In acute exposure, RR toxicity was expressed through an increase of the base level locomotor activities during light periods, while the dark-induced hyperactivity was usually abolished in dark periods, in chronic and acute exposures (RR samples and single toxicant exposures). Furthermore, for each type of exposure (acute or chronic), the effect was observed either in light or in dark condition. In addition, the absence of a statistically significant effect compared to control larvae observed during the light period for the C site in chronic exposure (Figure 1A–C) may possibly reflect the existence of stimulating and inhibiting effects that compensate each other, according to the different chemical concentrations and combination in the samples. The results obtained for the two consecutive samples from the C site (2017-06-27; 2017-06-28) did not reveal a decrease in the toxicity but merely different responses to dark–light stress (Figure 1B,C,E,F). Indeed, pollutants concentrations are often expected to decrease between rainfall events and within rainfalls, with most of the toxic load being released within the first few minutes (first flush). However, these samples had comparable concentrations of aliphatic hydrocarbons and PAHs, but differed by their phthalates and alkylphenols contents which were higher in the 2017-28-06 sample, and global parameters that were higher in the one of 2017-06-27, except DOC. Thus, the chemical analysis revealed a relative temporal variability between the two samples, which could account for the different larval responses to stress, and the absence of a “first flush” phenomenon. This temporal variability was confirmed by NTS results.

The HRMS analysis proved to be a valuable approach to complete the characterization of the RR samples realized by target screening and to detect site-specific or common toxicants. This approach allowed us to conclude that the heavy traffic site RR samples differed from samples collected from the moderate traffic road and that specific features could also occur due to temporal variations (as observed for the C site). The study of each site chromatographic fingerprints allowed the identification of peaks with important intensities. Among the most intense features detected from the C site in both ESI+ and ESI– modes, several identified compounds (DPG, 1,3-benzothiazole-2-sulfonic acid) originated from the composition of tires and could be related to the intensity of the traffic. We confirmed the presence of DPG in tire leachates through the non-target analysis of different commercial tires leachates. The greater presence of BZT observed in winter could be related to the application of deicing salts on the road at the C site during this period (January–March), which was confirmed by higher conductivity values. The presence of salt on the road could also facilitate the release of compounds from tires and explain the intense signals observed during winter. 6PPD leaching from tires was observed during the experiments

using simulated rainwater, confirming the potential release of 6PPD and risk of formation of 6PPD-quinone. Other nitrogen-containing molecules were tentatively identified from the leachates and detected in some of the RR samples, but they could not be found in other publications related to RR characterization or rubber manufacturing. More work would thus be needed to confirm their molecular structures and to assess their potential use as runoff markers in environmental samples as well as the associated risks. Collectively, from the results obtained with the light–dark stress test, the mitochondrial respiratory chain complex I assay, and those from non-target and target screening [9], it could be concluded that the RR samples contained a mix of pollutants differing both by their proportions and site-specific content, with potentially deleterious consequences in terms of ecotoxicological impacts, at least on the studied parameters.

Based on these findings, we selected DPG and BZT for analyses using the light–dark stress and complex I enzymatic assays. Few studies have been performed on DPG ecotoxicity, and limited data are available. As it has been shown that DPG slightly photolyzes but is generally not biodegradable and is also stable to hydrolysis [76], it was of interest to evaluate its ecotoxicological impact. OECD mentioned DPG to be toxic to fish ( $LC_{50}$  at 96 h = 4.2–11 mg/L, predicted non-effect concentration at 6  $\mu$ g/L) [77]. The toxicity of BZT and its derivatives was investigated on non-target organisms in several studies [78,79], including zebrafish ( $LC_{50}$  at 96h = 171 mg/L). These concentrations were far above those found at the C site, explaining why we did not record any mortality. Both molecules inhibited the distance moved by the larvae, showing that even sub-lethal concentrations could potentially jeopardize the larvae's survival. As DPG exposure revealed inhibition of the distance moved by the larvae at the low concentration, but not at the high one, DPG could potentially have a non-monotonic concentration-effect profile on behavior, although further studies are required to strengthen this hypothesis. Interestingly, such profiles have been observed for various physiological and behavioral effects involving endocrine disruptors, such as bisphenol A (BPA) and DEHP [80]. DPG, with its two benzene rings structure resembling BPA, could exhibit such endocrine disruption properties impacting behavior. Interestingly, the endocrine disruption effect of BZT has been described on marine medakas at 10  $\mu$ g/L, impacting the synthesis of estrogens [81], while it induced hepatotoxicity at 600  $\mu$ g/L on zebrafish exposed for 30 days, by apoptosis triggered by oxidative stress [82]. Furthermore, we obtained unexpected results with the DPG–BZT mixes, as both concentration combinations failed to inhibit larval activity compared to controls, highlighting the unpredictability of pollutant cocktails effects versus those of contaminants taken individually [83,84]. Noteworthy, Duan et al. reported that cadmium hepatotoxicity (1  $\mu$ M) was alleviated by the presence of BZT in adult zebrafish by the formation of Cd–BZT complexes, resulting in reduced apoptosis in the liver [82]. Although complete metals analysis could not be performed on all the samples, the occurrence of such interactions adds another level of complexity to the interpretation of toxicity data.

The chemicals' complexity and the multiplicity of their targets in the RR were further reinforced by the results of the complex I enzymatic assay. Mitochondria are intracellular organelles whose roles in energy production, steroids biosynthesis, reactive species of oxygen production are well established. Mitochondrial dysfunction leads to the alteration of important molecular mechanisms, which are implicated in the pathogenesis of numerous diseases such as cancer, neurodegenerative diseases, or diabetes [66]. It can result from environmental pollutants exposure (e.g., pesticides, herbicides, biocides, industrial and pharmaceutical compounds, etc.) even at low concentrations, which target the respiratory chain complexes and, in particular, the complex I (NADH-coenzyme Q oxidoreductase) [65]. As the major entry point for electrons into the respiratory chain, complex I plays a crucial role in regulating oxidative phosphorylation and mitochondrial respiration [85]. Thus, a decreased activity of this complex may alter the production of ATP and lead to oxidative stress, which in turn may contribute to tissue damage.

In the absence of literature on the impacts of RR chemicals on complex I activity (e.g., hydrocarbons, alkylphenols, per- and polyfluoroalkyl substances (PFAS), etc.), several

hypotheses can be drawn to explain the marked inhibiting effect on complex I activity at the R site: (i) The presence of chemical structure analogies between molecules involved in mitochondrial complex I function, petrochemicals or other industrial compounds present in the RR and classical inhibitors of complex I could explain the inhibition observed. Indeed, this sample contained various alkylphenols (Table 2) with a related chemical structure to synthetic derivatives from capsaicin, which have been shown to inhibit complex I [86].

(ii) Interestingly, a sample collected (2017-06-29) two months before at the R site presented unexpectedly high concentrations in perfluorinated compounds, including perfluorooctanoic acid (PFOA)—a widely used industrial surfactant—(120.7 ng/L). The 2 preceding samples (2016-11-22; 2017-03-23) concentrations were 40.9 ng/L and 10.1 ng/L, respectively. Although this analysis has not been performed on the 2017-09-14 sample, it is likely that PFOA would have still been detectable given its known persistence in the environment [87,88]. Its presence at the R site has been hypothesized to be linked to construction work in the neighborhood at the sampling time and to illegal dumping of construction waste in the sewer system. Furthermore, some fluorinated compounds (ethyl-4,4,4-trifluoro-3-hydroxybutanoate and 1-(2,2-difluoroethoxy)-3-decanol) were identified by HRMS in the sample from the R site (2018-03-29), which further reinforces this hypothesis. PFOA has been shown to inhibit complex I activity of brain and liver rat mitochondria, a mechanism that has been hypothesized to participate in driving adverse effects in animal models [89] and in humans [90]. This inhibition was associated with an increased reactive oxygen species production, peroxidation of mitochondrial membrane, a decrease in ATP production, and a release of cytochrom c, normally leading to programmed cell death (apoptosis). Thus, PFOA, presumably present in the R site samples, could possibly participate in the observed inhibition of complex I activity. It should be noted that the perfluorinated compounds have not been analyzed in the C site samples in 2017 and their concentrations were below the quantification limit when performed in 2016 (4 samples).

By comparison, RR at the C site did not produce a significant inhibition of complex I activity, although containing DPG and, to a lesser extent, BZT. This likely suggests that among the mixture of molecules in this RR, some may interfere in the enzymatic assay, possibly by a detergent effect modifying the tridimensional organization of the complex I different subunits [91] or competing for the same binding sites, thus resulting in the loss of the inhibitory effect. Indeed, several groups of alkylphenols (octylphenols; nonylphenols), present in the RR dissolved phase at much greater concentrations at the C site than at the R site (e.g., nonylphenol monoethoxylate (NP1EO), 858 ng/L vs. 132 ng/L; 4-tert octylphenol (OP), 114 ng/L vs. 52 ng/L; nonylphenol monoethoxy-carboxylate (NP1EC) 103 ng/L vs. 49 ng/L), are used as detergents or enter in the manufacturing process of tires (reviewed in [92]).

We also show, for the first time to our best knowledge, that DPG identified by NTS inhibited complex I activity. Several hypotheses might be considered to explain this inhibition. (i) As mentioned above, DPG has a chemical structure related to BPA, which has also been reported to inhibit complex I [93]. (ii) Furthermore, because of its long-known antioxidant properties [94], it may interfere with the electron transfer along the respiratory chain complexes, the reduction of ubiquinone in ubiquinol, and induce the production of superoxide anion at the complex I level [95]. Given the design of our assay, which uses complex III activity as a reporter, it cannot be ruled out that it may, in addition, interfere with this complex, where similar types of reactions take place. (iii) Finally, knowing its role as an accelerator in the sulfur vulcanization process, it can react with sulfur by its amine group [96] to produce free radicals causing rubber to be structured. Although mitochondrial physiological conditions are obviously very distant from those during vulcanization, it is not inconceivable that DPG might potentially interact with and perturbate complexes I and III, which hold Fe/S clusters in their structure.

## 5. Conclusions

In conclusion, the study of two sites differing by their traffic intensities revealed that this difference could be evidenced at the molecular level by combining physico-chemical analyses, 3D fluorescence, and target/non-target screenings. This original top-down approach (from complex samples to single molecules) represents an effective way of characterizing complex environmental contaminants mixtures. Establishing specific environmental HRMS signatures is still an emerging, promising but challenging strategy to classify urban chemical sources and poorly documented to date [14,15]. Even fewer studies coupled HRMS and toxicological analysis, for example, applied to the detection of contaminants in RR-exposed fish tissues [16], or ecotoxicological assessment, leading for instance to the identification of a highly toxic quinone transformation product of 6PPD for coho salmon [72]. Such effect-directed analysis approaches, increasingly followed, are very effective for the identification of specific toxicants ([97], and references therein). Further insights about the composition of samples can be obtained through the concomitant characterization of DOM by 3D fluorescence, the diversity of pollutants by NTS, and their concentrations by targeted analyses. These can provide valuable complementary information, especially when comparing samples. In our work, quantitative data obtained by target screening were expected to demonstrate a relationship between the concentration of micropollutants and the intensity of traffic [9], which was indeed suggested by the characterization of DOM fluorophores. However, the ranges of concentrations obtained from the targeted analyses of samples selected in our study were similar between the two sites. In contrast, HRMS revealed specific fingerprints of both sites. Overall, these differences may provide some potential clues on why samples from both sites showed different toxicity profiles.

HRMS fingerprints of both RR and tire leachates allowed the identification of several toxicants that had not been specifically searched by targeted screening. We subsequently assessed the toxic potential of the RR samples and of two specific compounds (DPG and BZT) revealed by the HRMS analysis. The behavioral test on zebrafish embryos and the enzymatic test of the mitochondrial respiratory chain showed that sublethal concentrations of these compounds (alone or in mixtures) and those present in the RR can still have deleterious effects on aquatic organisms.

Our findings have highlighted the need and the relevance of such a strategy combining biological tests and state-of-the-art chemical analysis techniques for a comprehensive risk evaluation of complex environmental samples, such as road runoff, and the design of efficient depolluting devices such as sustainable drainage systems. Furthermore, it paves the way towards a systematic and adaptable approach towards other types of matrices, e.g., urban domestic wastewater or surface water.

**Supplementary Materials:** The following are available online at <https://www.mdpi.com/article/10.3390/w14040511/s1>, Figure S1: 3D fluorescence indexes for all road runoff samples; Figure S2: HRMS fingerprints of road runoff samples (C = Compans, R = Rosny-sous-Bois). The size of bubbles is proportional to the intensity of the feature, and intensities are normalized by the highest intensity of each sample (i.e., all fingerprints get the same range of intensities); Figure S3: HRMS fingerprints of road runoff samples (C = Compans, R = Rosny-sous-Bois): comparison between C 2017-03-01 and R 2018-03-29 samples. The size of bubbles is proportional to the intensity of the feature; Figure S4: Boxplots representing the intensities of benzotriazole in each sample (triplicate injections in ESI+ mode). C = Compans; R = Rosny; Figure S5: Boxplots representing the intensities of 1,3-benzothiazole-2-sulfonic acid in each sample (triplicate injections in ESI− mode). C = Compans; R = Rosny; Figure S6: HRMS fingerprints of tire leachates (features with intensity values higher than 6000), obtained with (a) simulated rainwater and (b) methanol. The size of bubbles is proportional to the area of the feature; Table S1: Specific features tentatively identified by NTS at each site; Table S2: Features tentatively identified by NTS in the tire leachates.



**Author Contributions:** Methodology, investigation, data curation, visualization, F.S., N.H., G.V. and C.M.; writing—original draft preparation, F.S. and N.H.; formal analysis, G.V., C.M., R.M., J.L.R. and L.G.-A.; supervision, validation, writing—review and editing, J.L.R. and L.G.-A.; conceptualization, resources, project administration, funding acquisition, writing—review and editing, M.-C.G. All authors have read and agreed to the published version of the manuscript.

**Funding:** This research was part of the ROULÉPUR research project funded by Agence de l'Eau Seine Normandie and Office Français de la Biodiversité.

**Data Availability Statement:** The full data set of concentrations for target screening will be made available as a repository on Mendeley Data, V1, doi:10.17632/m8kcmthfd2.1. The raw HRMS data files are available at doi:10.5281/zenodo.4306663.

**Acknowledgments:** This study has been conducted within the framework of the Observatory of Urban Pollutants in Paris (OPUR). We thank all partners and collaborators of the ROULÉPUR project: K. Flanagan, M. Saad, and J. Paupardin for the sampling campaign management in Compans and Rosny; the Seine-et-Marne and Seine-Saint-Denis Departmental Councils for their partnership and technical support. We also acknowledge the PRAMMICS Platform (OSU-EFLUVE UMS 3563) for the access to HRMS and Zembrax instruments, and especially Emmanuelle Mebold for her technical support on HRMS instruments.

**Conflicts of Interest:** The authors declare no conflict of interest. The funders had no role in the design of the study; in the collection, analyses, or interpretation of data; in the writing of the manuscript, or in the decision to publish the results.

## References

1. Gasperi, J.; Sebastian, C.; Ruban, V.; Delamain, M.; Percot, S.; Wiest, L.; Mirande, C.; Caupos, E.; Demare, D.; Kessoo, M.D.K.; et al. Micropollutants in Urban Stormwater: Occurrence, Concentrations, and Atmospheric Contributions for a Wide Range of Contaminants in Three French Catchments. *Environ. Sci. Pollut. Res. Int.* **2014**, *21*, 5267–5281. [\[CrossRef\]](#)
2. Revitt, D.M.; Lundy, L.; Coulon, F.; Fairley, M. The Sources, Impact and Management of Car Park Runoff Pollution: A Review. *J. Environ. Manag.* **2014**, *146*, 552–567. [\[CrossRef\]](#)
3. Markiewicz, A.; Björklund, K.; Eriksson, E.; Kalmykova, Y.; Strömvall, A.-M.; Siopi, A. Emissions of Organic Pollutants from Traffic and Roads: Priority Pollutants Selection and Substance Flow Analysis. *Sci. Total Environ.* **2017**, *580*, 1162–1174. [\[CrossRef\]](#) [\[PubMed\]](#)
4. Amorello, D.; Barreca, S.; Orecchio, S.; Ferro, S. Platinum in Indoor Settled Dust Matter (Homes and Cars). *Microchem. J.* **2015**, *123*, 76–83. [\[CrossRef\]](#)
5. Orecchio, S.; Amorello, D.; Barreca, S.; Valenti, A. Wood Pellets for Home Heating Can Be Considered Environmentally Friendly Fuels? Polycyclic Aromatic Hydrocarbons (PAHs) in Their Ashes. *Microchem. J.* **2016**, *124*, 267–271. [\[CrossRef\]](#)
6. Orecchio, S.; Amorello, D.; Barreca, S. (II) Wood Pellets for Home Heating Can Be Considered Environmentally Friendly Fuels? Heavy Metals Determination by Inductively Coupled Plasma-Optical Emission Spectrometry (ICP-OES) in Their Ashes and the Health Risk Assessment for the Operators. *Microchem. J.* **2016**, *127*, 178–183. [\[CrossRef\]](#)
7. Eriksson, E.; Baun, A.; Scholes, L.; Ledin, A.; Ahlman, S.; Revitt, M.; Noutsopoulos, C.; Mikkelsen, P.S. Selected Stormwater Priority Pollutants—A European Perspective. *Sci. Total Environ.* **2007**, *383*, 41–51. [\[CrossRef\]](#)
8. Wagner, S.; Hüffer, T.; Klöckner, P.; Wehrhahn, M.; Hofmann, T.; Reemtsma, T. Tire Wear Particles in the Aquatic Environment—A Review on Generation, Analysis, Occurrence, Fate and Effects. *Water Res.* **2018**, *139*, 83–100. [\[CrossRef\]](#)
9. Gasperi, J.; Le Roux, J.; Deshayes, S.; Ayrault, S.; Bordier, L.; Boudahmane, L.; Budzinski, H.; Caupos, E.; Caubrière, N.; Flanagan, K.; et al. Micropollutants in the Urban Runoff from Traffic Areas: Target and Non-Target Screening on Four Contrasted Sites. *Water* **2022**, *14*, 394. [\[CrossRef\]](#)
10. Bressy, A.; Gromaire, M.-C.; Lorgeoux, C.; Chebbo, G. Alkylphenols in Atmospheric Depositions and Urban Runoff. *Water Sci. Technol.* **2011**, *63*, 671–679. [\[CrossRef\]](#)
11. Bressy, A.; Gromaire, M.-C.; Lorgeoux, C.; Saad, M.; Leroy, F.; Chebbo, G. Towards the Determination of an Optimal Scale for Stormwater Quality Management: Micropollutants in a Small Residential Catchment. *Water Res.* **2012**, *46*, 6799–6810. [\[CrossRef\]](#) [\[PubMed\]](#)
12. Krauss, M.; Singer, H.; Hollender, J. LC-High Resolution MS in Environmental Analysis: From Target Screening to the Identification of Unknowns. *Anal. Bioanal. Chem.* **2010**, *397*, 943–951. [\[CrossRef\]](#)
13. Schymanski, E.L.; Singer, H.P.; Slobodnik, J.; Ipolyi, I.M.; Oswald, P.; Krauss, M.; Schulze, T.; Haglund, P.; Letzel, T.; Grosse, S.; et al. Non-Target Screening with High-Resolution Mass Spectrometry: Critical Review Using a Collaborative Trial on Water Analysis. *Anal. Bioanal. Chem.* **2015**, *407*, 6237–6255. [\[CrossRef\]](#) [\[PubMed\]](#)
14. Du, B.; Tian, Z.; Peter, K.T.; Kolodziej, E.P.; Wong, C.S. Developing Unique Nontarget High-Resolution Mass Spectrometry Signatures to Track Contaminant Sources in Urban Waters. *Environ. Sci. Technol. Lett.* **2020**, *7*, 923–930. [\[CrossRef\]](#) [\[PubMed\]](#)

15. Seiwert, B.; Klöckner, P.; Wagner, S.; Reemtsma, T. Source-Related Smart Suspect Screening in the Aqueous Environment: Search for Tire-Derived Persistent and Mobile Trace Organic Contaminants in Surface Waters. *Anal. Bioanal. Chem.* **2020**, *412*, 4909–4919. [\[CrossRef\]](#)
16. Du, B.; Lofton, J.M.; Peter, K.T.; Gipe, A.D.; James, C.A.; McIntyre, J.K.; Scholz, N.L.; Baker, J.E.; Kolodziej, E.P. Development of Suspect and Non-Target Screening Methods for Detection of Organic Contaminants in Highway Runoff and Fish Tissue with High-Resolution Time-of-Flight Mass Spectrometry. *Environ. Sci.: Process. Impacts* **2017**, *19*, 1185–1196. [\[CrossRef\]](#)
17. Robinson, P.D. Behavioural Toxicity of Organic Chemical Contaminants in Fish: Application to Ecological Risk Assessments (ERAs). *Can. J. Fish. Aquat. Sci.* **2009**, *66*, 1179–1188. [\[CrossRef\]](#)
18. Linbo, T.L.; Baldwin, D.H.; McIntyre, J.K.; Scholz, N.L. Effects of Water Hardness, Alkalinity, and Dissolved Organic Carbon on the Toxicity of Copper to the Lateral Line of Developing Fish. *Environ. Toxicol. Chem.* **2009**, *28*, 1455–1461. [\[CrossRef\]](#)
19. Wernersson, A.-S.; Carere, M.; Maggi, C.; Tusil, P.; Soldan, P.; James, A.; Sanchez, W.; Dulio, V.; Broeg, K.; Reifferscheid, G.; et al. The European Technical Report on Aquatic Effect-Based Monitoring Tools under the Water Framework Directive. *Environ. Sci. Eur.* **2015**, *27*, 7. [\[CrossRef\]](#)
20. Ginebreda, A.; Kuzmanovic, M.; Guasch, H.; de Alda, M.L.; López-Doval, J.C.; Muñoz, I.; Ricart, M.; Romani, A.M.; Sabater, S.; Barceló, D. Assessment of Multi-Chemical Pollution in Aquatic Ecosystems Using Toxic Units: Compound Prioritization, Mixture Characterization and Relationships with Biological Descriptors. *Sci. Total Environ.* **2014**, *468–469*, 715–723. [\[CrossRef\]](#)
21. Prasse, C.; Stalter, D.; Schulte-Oehlmann, U.; Oehlmann, J.; Ternes, T.A. Spoilt for Choice: A Critical Review on the Chemical and Biological Assessment of Current Wastewater Treatment Technologies. *Water Res.* **2015**, *87*, 237–270. [\[CrossRef\]](#) [\[PubMed\]](#)
22. Neale, P.A.; Altenburger, R.; Ait-Aïssa, S.; Brion, F.; Busch, W.; de Aragão Umbuzeiro, G.; Denison, M.S.; Du Pasquier, D.; Hilscherová, K.; Hollert, H.; et al. Development of a Bioanalytical Test Battery for Water Quality Monitoring: Fingerprinting Identified Micropollutants and Their Contribution to Effects in Surface Water. *Water Res.* **2017**, *123*, 734–750. [\[CrossRef\]](#) [\[PubMed\]](#)
23. Tousova, Z.; Oswald, P.; Slobodnik, J.; Blaha, L.; Muz, M.; Hu, M.; Brack, W.; Krauss, M.; Di Paolo, C.; Tarcai, Z.; et al. European Demonstration Program on the Effect-Based and Chemical Identification and Monitoring of Organic Pollutants in European Surface Waters. *Sci. Total Environ.* **2017**, *601–602*, 1849–1868. [\[CrossRef\]](#) [\[PubMed\]](#)
24. Hill, A.J.; Teraoka, H.; Heideman, W.; Peterson, R.E. Zebrafish as a Model Vertebrate for Investigating Chemical Toxicity. *Toxicol. Sci.* **2005**, *86*, 6–19. [\[CrossRef\]](#) [\[PubMed\]](#)
25. He, J.-H.; Gao, J.-M.; Huang, C.-J.; Li, C.-Q. Zebrafish Models for Assessing Developmental and Reproductive Toxicity. *Neurotoxicol. Teratol.* **2014**, *42*, 35–42. [\[CrossRef\]](#)
26. McCollum, C.W.; Ducharme, N.A.; Bondesson, M.; Gustafsson, J.-A. Developmental Toxicity Screening in Zebrafish. *Birth Defects Res. Part C Embryo Today Rev.* **2011**, *93*, 67–114. [\[CrossRef\]](#)
27. Mione, M.C.; Trede, N.S. The Zebrafish as a Model for Cancer. *Dis. Model. Mech.* **2010**, *3*, 517–523. [\[CrossRef\]](#)
28. Bai, Q.; Burton, E.A. Zebrafish Models of Tauopathy. *Biochim. Biophys. Acta* **2011**, *1812*, 353–363. [\[CrossRef\]](#)
29. Goldsmith, J.R.; Jobin, C. Think Small: Zebrafish as a Model System of Human Pathology. *J. Biomed. Biotechnol.* **2012**, *2012*, e817341. [\[CrossRef\]](#)
30. Chávez, M.N.; Aedo, G.; Fierro, F.A.; Allende, M.L.; Egaña, J.T. Zebrafish as an Emerging Model Organism to Study Angiogenesis in Development and Regeneration. *Front. Physiol.* **2016**, *7*, 56. [\[CrossRef\]](#)
31. Scott, G.R.; Sloman, K.A. The Effects of Environmental Pollutants on Complex Fish Behaviour: Integrating Behavioural and Physiological Indicators of Toxicity. *Aquat. Toxicol.* **2004**, *68*, 369–392. [\[CrossRef\]](#) [\[PubMed\]](#)
32. Selderslaghs, I.W.T.; Hooyberghs, J.; Blust, R.; Witters, H.E. Assessment of the Developmental Neurotoxicity of Compounds by Measuring Locomotor Activity in Zebrafish Embryos and Larvae. *Neurotoxicol. Teratol.* **2013**, *37*, 44–56. [\[CrossRef\]](#)
33. Legradi, J.B.; Di Paolo, C.; Kraak, M.H.S.; van der Geest, H.G.; Schymanski, E.L.; Williams, A.J.; Dingemans, M.M.L.; Massei, R.; Brack, W.; Cousin, X.; et al. An Ecotoxicological View on Neurotoxicity Assessment. *Environ. Sci. Eur.* **2018**, *30*, 46. [\[CrossRef\]](#) [\[PubMed\]](#)
34. Ogungbemi, A.; Leuthold, D.; Scholz, S.; Küster, E. Hypo- or Hyperactivity of Zebrafish Embryos Provoked by Neuroactive Substances: A Review on How Experimental Parameters Impact the Predictability of Behavior Changes. *Environ. Sci. Eur.* **2019**, *31*, 88. [\[CrossRef\]](#)
35. Young, A.; Kochenkov, V.; McIntyre, J.K.; Stark, J.D.; Coffin, A.B. Urban Stormwater Runoff Negatively Impacts Lateral Line Development in Larval Zebrafish and Salmon Embryos. *Sci. Rep.* **2018**, *8*, 2830. [\[CrossRef\]](#) [\[PubMed\]](#)
36. McIntyre, J.K.; Edmunds, R.C.; Redig, M.G.; Mudrock, E.M.; Davis, J.W.; Incardona, J.P.; Stark, J.D.; Scholz, N.L. Confirmation of Stormwater Bioretention Treatment Effectiveness Using Molecular Indicators of Cardiovascular Toxicity in Developing Fish. *Environ. Sci. Technol.* **2016**, *50*, 1561–1569. [\[CrossRef\]](#)
37. Wu, L.; Jiang, Y.; Zhang, L.; Chen, L.; Zhang, H. Toxicity of Urban Highway Runoff in Shanghai to Zebrafish (*Danio Rerio*) Embryos and Luminous Bacteria (*Vibrio Qinghaiensis* Q67). *Environ. Sci. Pollut. Res. Int.* **2014**, *21*, 2663–2676. [\[CrossRef\]](#)
38. Chen, X.D.; Culbert, E.; Hebert, V.; Stark, J.D. Mixture Effects of the Nonylphenyl Polyethoxylate, R-11 and the Insecticide, Imidacloprid on Population Growth Rate and Other Parameters of the Crustacean, *Ceriodaphnia Dubia*. *Ecotoxicol. Environ. Saf.* **2010**, *73*, 132–137. [\[CrossRef\]](#)
39. Chen, H.; Yao, J.; Wang, F.; Zhou, Y.; Chen, K.; Zhuang, R.; Choi, M.M.F.; Zaray, G. Toxicity of Three Phenolic Compounds and Their Mixtures on the Gram-Positive Bacteria *Bacillus Subtilis* in the Aquatic Environment. *Sci. Total Environ.* **2010**, *408*, 1043–1049. [\[CrossRef\]](#)

40. Shao, Y.; Chen, Z.; Hollert, H.; Zhou, S.; Deutschmann, B.; Seiler, T.-B. Toxicity of 10 Organic Micropollutants and Their Mixture: Implications for Aquatic Risk Assessment. *Sci. Total Environ.* **2019**, *666*, 1273–1282. [\[CrossRef\]](#)
41. Peng, X.; Lin, J.; Zhu, Y.; Liu, X.; Zhang, Y.; Ji, Y.; Yang, X.; Zhang, Y.; Guo, N.; Li, Q. Anxiety-Related Behavioral Responses of Pentylene-tetrazole-Treated Zebrafish Larvae to Light-Dark Transitions. *Pharm. Biochem. Behav.* **2016**, *145*, 55–65. [\[CrossRef\]](#)
42. Leuthold, D.; Klüver, N.; Altenburger, R.; Busch, W. Can Environmentally Relevant Neuroactive Chemicals Specifically Be Detected with the Locomotor Response Test in Zebrafish Embryos? *Environ. Sci. Technol.* **2019**, *53*, 482–493. [\[CrossRef\]](#) [\[PubMed\]](#)
43. Flanagan, K.; Branchu, P.; Boudahmane, L.; Caupos, E.; Demare, D.; Deshayes, S.; Dubois, P.; Meffray, L.; Partibane, C.; Saad, M.; et al. Field Performance of Two Biofiltration Systems Treating Micropollutants from Road Runoff. *Water Res.* **2018**, *145*, 562–578. [\[CrossRef\]](#) [\[PubMed\]](#)
44. Flanagan, K.; Branchu, P.; Boudahmane, L.; Caupos, E.; Demare, D.; Deshayes, S.; Dubois, P.; Meffray, L.; Partibane, C.; Saad, M.; et al. Retention and Transport Processes of Particulate and Dissolved Micropollutants in Stormwater Biofilters Treating Road Runoff. *Sci. Total Environ.* **2019**, *656*, 1178–1190. [\[CrossRef\]](#) [\[PubMed\]](#)
45. Alberts, J.J.; Takács, M. Total Luminescence Spectra of IHSS Standard and Reference Fulvic Acids, Humic Acids and Natural Organic Matter: Comparison of Aquatic and Terrestrial Source Terms. *Org. Geochem.* **2004**, *35*, 243–256. [\[CrossRef\]](#)
46. Lawaetz, A.J.; Stedmon, C.A. Fluorescence Intensity Calibration Using the Raman Scatter Peak of Water. *Appl. Spectrosc.* **2009**, *63*, 936–940. [\[CrossRef\]](#)
47. Parlanti, E. Dissolved Organic Matter Fluorescence Spectroscopy as a Tool to Estimate Biological Activity in a Coastal Zone Submitted to Anthropogenic Inputs. *Org. Geochem.* **2000**, *31*, 1765–1781. [\[CrossRef\]](#)
48. Zsolnay, A.; Baigar, E.; Jimenez, M.; Steinweg, B.; Saccomandi, F. Differentiating with Fluorescence Spectroscopy the Sources of Dissolved Organic Matter in Soils Subjected to Drying. *Chemosphere* **1999**, *38*, 45–50. [\[CrossRef\]](#)
49. Huguet, A.; Vacher, L.; Relexans, S.; Saubusse, S.; Froidefond, J.M.; Parlanti, E. Properties of Fluorescent Dissolved Organic Matter in the Gironde Estuary. *Org. Geochem.* **2009**, *40*, 706–719. [\[CrossRef\]](#)
50. Lamprea, K.; Bressy, A.; Mirande-Bret, C.; Caupos, E.; Gromaire, M.-C. Alkylphenol and Bisphenol A Contamination of Urban Runoff: An Evaluation of the Emission Potentials of Various Construction Materials and Automotive Supplies. *Environ. Sci. Pollut. Res.* **2018**, *25*, 21887–21900. [\[CrossRef\]](#)
51. Van De Voorde, A. Incidence of Roof Maintenance Practices on the Quality of Runoff Water. Case of Biocidal Treatment Products. Ph.D. Thesis, Université Paris Est, Paris, France, June 2012.
52. Huynh, N.; Caupos, E.; Soares Peirera, C.; Le Roux, J.; Bressy, A.; Moilleron, R. Evaluation of Sample Preparation Methods for Non-Target Screening of Organic Micropollutants in Urban Waters Using High-Resolution Mass Spectrometry. *Molecules* **2021**, *26*, 7064. [\[CrossRef\]](#) [\[PubMed\]](#)
53. Rosnack, K.J.; Reid, M.J.; Ladak, A.; Cleland, G. Screening Solution Using the Software Platform UNIFI: An Integrated Workflow by Waters. In *Assessing Transformation Products of Chemicals by Non-Target and Suspect Screening—Strategies and Workflows Volume 2*; ACS Symposium Series; American Chemical Society: Washington, DC, USA, 2016; Volume 1242, pp. 155–172, ISBN 978-0-8412-3195-5.
54. R Core Team. *R: A Language and Environment for Statistical Computing*, v.3.6.2; R Foundation for Statistical Computing: Vienna, Austria, 2020.
55. Schlager, S. Morpho and Rvcg—Shape Analysis in R. In *Statistical Shape and Deformation Analysis*; Zheng, G., Li, S., Székely, G., Eds.; Academic Press: Cambridge, MA, USA, 2017; pp. 217–256, ISBN 978-0-12-810493-4.
56. Kassambara, A.; Mundt, F. *Factoextra: Extract and Visualize the Results of Multivariate Data Analyses*; R Foundation for Statistical Computing: Vienna, Austria, 2020.
57. Sievert, C. *Interactive Web-Based Data Visualization with R, Plotly, and Shiny*; Chapman and Hall/CRC: Boca Raton, FL, USA, 2020; ISBN 978-1-138-33145-7.
58. Council of the European Union. Directive 2010/63/EU of the European Parliament and of the Council of 22 September 2010 on the Protection of Animals Used for Scientific Purposes. Available online: <https://eur-lex.europa.eu/legal-content/EN/TXT/PDF/?uri=CELEX:32010L0063> (accessed on 26 December 2021).
59. Hernandez, R.E.; Galitan, L.; Cameron, J.; Goodwin, N.; Ramakrishnan, L. Delay of Initial Feeding of Zebrafish Larvae Until 8 Days Postfertilization Has No Impact on Survival or Growth Through the Juvenile Stage. *Zebrafish* **2018**, *15*, 515–518. [\[CrossRef\]](#) [\[PubMed\]](#)
60. Strähle, U.; Scholz, S.; Geisler, R.; Greiner, P.; Hollert, H.; Rastegar, S.; Schumacher, A.; Selderslaghs, I.; Weiss, C.; Witters, H.; et al. Zebrafish Embryos as an Alternative to Animal Experiments—A Commentary on the Definition of the Onset of Protected Life Stages in Animal Welfare Regulations. *Reprod. Toxicol.* **2012**, *33*, 128–132. [\[CrossRef\]](#)
61. Kimmel, C.B.; Ballard, W.W.; Kimmel, S.R.; Ullmann, B.; Schilling, T.F. Stages of Embryonic Development of the Zebrafish. *Dev. Dyn.* **1995**, *203*, 253–310. [\[CrossRef\]](#) [\[PubMed\]](#)
62. Cormier, A.; Morin, C.; Zini, R.; Tillement, J.-P.; Lagrue, G. Nicotine Protects Rat Brain Mitochondria against Experimental Injuries. *Neuropharmacology* **2003**, *44*, 642–652. [\[CrossRef\]](#)
63. Zhou, S.; Chen, Q.; Di Paolo, C.; Shao, Y.; Hollert, H.; Seiler, T.-B. Behavioral Profile Alterations in Zebrafish Larvae Exposed to Environmentally Relevant Concentrations of Eight Priority Pharmaceuticals. *Sci. Total Environ.* **2019**, *664*, 89–98. [\[CrossRef\]](#)
64. Guo, N.; Lin, J.; Peng, X.; Chen, H.; Zhang, Y.; Liu, X.; Li, Q. Influences of Acute Ethanol Exposure on Locomotor Activities of Zebrafish Larvae under Different Illumination. *Alcohol* **2015**, *49*, 727–737. [\[CrossRef\]](#)



65. Degli Esposti, M. Inhibitors of NADH-Ubiquinone Reductase: An Overview. *Biochim. Biophys. Acta* **1998**, *1364*, 222–235. [[CrossRef](#)]
66. Meyer, J.N.; Leung, M.C.K.; Rooney, J.P.; Sendoel, A.; Hengartner, M.O.; Kisby, G.E.; Bess, A.S. Mitochondria as a Target of Environmental Toxicants. *Toxicol. Sci.* **2013**, *134*, 1–17. [[CrossRef](#)]
67. Hughey, C.A.; Hendrickson, C.L.; Rodgers, R.P.; Marshall, A.G.; Qian, K. Kendrick Mass Defect Spectrum: A Compact Visual Analysis for Ultrahigh-Resolution Broadband Mass Spectra. *Anal. Chem.* **2001**, *73*, 4676–4681. [[CrossRef](#)]
68. Thurman, E.M.; Ferrer, I.; Blotvogel, J.; Borch, T. Analysis of Hydraulic Fracturing Flowback and Produced Waters Using Accurate Mass: Identification of Ethoxylated Surfactants. *Anal. Chem.* **2014**, *86*, 9653–9661. [[CrossRef](#)]
69. Hinnenkamp, V.; Balsaa, P.; Schmidt, T.C. Target, Suspect and Non-Target Screening Analysis from Wastewater Treatment Plant Effluents to Drinking Water Using Collision Cross Section Values as Additional Identification Criterion. *Anal. Bioanal. Chem.* **2021**, *414*, 425–438. [[CrossRef](#)]
70. Schulze, S.; Zahn, D.; Montes, R.; Rodil, R.; Quintana, J.B.; Knepper, T.P.; Reemtsma, T.; Berger, U. Occurrence of Emerging Persistent and Mobile Organic Contaminants in European Water Samples. *Water Res.* **2019**, *153*, 80–90. [[CrossRef](#)] [[PubMed](#)]
71. Challis, J.K.; Popick, H.; Prajapati, S.; Harder, P.; Giesy, J.P.; McPhedran, K.; Brinkmann, M. Occurrences of Tire Rubber-Derived Contaminants in Cold-Climate Urban Runoff. *Environ. Sci. Technol. Lett.* **2021**, *8*, 961–967. [[CrossRef](#)]
72. Tian, Z.; Zhao, H.; Peter, K.T.; Gonzalez, M.; Wetzel, J.; Wu, C.; Hu, X.; Prat, J.; Mudrock, E.; Hettinger, R.; et al. A Ubiquitous Tire Rubber-Derived Chemical Induces Acute Mortality in Coho Salmon. *Science* **2021**, *371*, 185–189. [[CrossRef](#)]
73. Farré, M.L.; Pérez, S.; Kantiani, L.; Barceló, D. Fate and Toxicity of Emerging Pollutants, Their Metabolites and Transformation Products in the Aquatic Environment. *TrAC Trends Anal. Chem.* **2008**, *27*, 991–1007. [[CrossRef](#)]
74. Tran, C.M.; Do, T.N.; Kim, K.-T. Comparative Analysis of Neurotoxicity of Six Phthalates in Zebrafish Embryos. *Toxics* **2021**, *9*, 5. [[CrossRef](#)] [[PubMed](#)]
75. Qian, L.; Liu, J.; Lin, Z.; Chen, X.; Yuan, L.; Shen, G.; Yang, W.; Wang, D.; Huang, Y.; Pang, S.; et al. Evaluation of the Spinal Effects of Phthalates in a Zebrafish Embryo Assay. *Chemosphere* **2020**, *249*, 126144. [[CrossRef](#)] [[PubMed](#)]
76. Zahn, D.; Mucha, P.; Zilles, V.; Touffet, A.; Gallard, H.; Knepper, T.P.; Frömel, T. Identification of Potentially Mobile and Persistent Transformation Products of REACH-Registered Chemicals and Their Occurrence in Surface Waters. *Water Res.* **2019**, *150*, 86–96. [[CrossRef](#)]
77. OECD. *Screening Information Dataset—Initial Assessment Report—1,3-Diphenylguanidine*; OECD: Paris, France, 2002.
78. Damalas, D.E.; Bletsou, A.A.; Agalou, A.; Beis, D.; Thomaidis, N.S. Assessment of the Acute Toxicity, Uptake and Biotransformation Potential of Benzotriazoles in Zebrafish (Danio Rerio) Larvae Combining HILIC- with RPLC-HRMS for High-Throughput Identification. *Environ. Sci. Technol.* **2018**, *52*, 6023–6031. [[CrossRef](#)] [[PubMed](#)]
79. Shi, Z.-Q.; Liu, Y.-S.; Xiong, Q.; Cai, W.-W.; Ying, G.-G. Occurrence, Toxicity and Transformation of Six Typical Benzotriazoles in the Environment: A Review. *Sci. Total Environ.* **2019**, *661*, 407–421. [[CrossRef](#)] [[PubMed](#)]
80. Lagarde, F.; Beausoleil, C.; Belcher, S.M.; Belzunces, L.P.; Emond, C.; Guerbet, M.; Rousselle, C. Non-Monotonic Dose-Response Relationships and Endocrine Disruptors: A Qualitative Method of Assessment. *Environ. Health* **2015**, *14*, 13. [[CrossRef](#)] [[PubMed](#)]
81. Tangtian, H.; Bo, L.; Wenhua, L.; Shin, P.K.S.; Wu, R.S.S. Estrogenic Potential of Benzotriazole on Marine Medaka (*Oryzias Melastigma*). *Ecotoxicol. Environ. Saf.* **2012**, *80*, 327–332. [[CrossRef](#)]
82. Duan, Z.; Xing, Y.; Feng, Z.; Zhang, H.; Li, C.; Gong, Z.; Wang, L.; Sun, H. Hepatotoxicity of Benzotriazole and Its Effect on the Cadmium Induced Toxicity in Zebrafish Danio Rerio. *Environ. Pollut.* **2017**, *224*, 706–713. [[CrossRef](#)] [[PubMed](#)]
83. Porseryd, T.; Kellner, M.; Reyhanian Caspillo, N.; Volkova, K.; Elabbas, L.; Ullah, S.; Olsén, H.; Dinné, P.; Porsch Hällström, I. Combinatory Effects of Low Concentrations of 17 $\alpha$ -Ethinylestradiol and Citalopram on Non-Reproductive Behavior in Adult Zebrafish (Danio Rerio). *Aquat. Toxicol.* **2017**, *193*, 9–17. [[CrossRef](#)]
84. Kinch, C.D.; Kurrasch, D.M.; Habibi, H.R. Adverse Morphological Development in Embryonic Zebrafish Exposed to Environmental Concentrations of Contaminants Individually and in Mixture. *Aquat. Toxicol.* **2016**, *175*, 286–298. [[CrossRef](#)]
85. Sharma, L.K.; Lu, J.; Bai, Y. Mitochondrial Respiratory Complex I: Structure, Function and Implication in Human Diseases. *Curr. Med. Chem.* **2009**, *16*, 1266–1277. [[CrossRef](#)]
86. Satoh, T.; Miyoshi, H.; Sakamoto, K.; Iwamura, H. Comparison of the Inhibitory Action of Synthetic Capsaicin Analogues with Various NADH-Ubiquinone Oxidoreductases. *Biochim. Biophys. Acta* **1996**, *1273*, 21–30. [[CrossRef](#)]
87. OECD/UNEP Global PFC Group. *Synthesis Paper on Per- and Polyfluorinated Chemicals (PFCs)*; OECD: Paris, France, 2013.
88. Savoca, D.; Melfi, R.; Palumbo Piccionello, A.; Barreca, S.; Buscemi, S.; Arizza, V.; Arculeo, M.; Pace, A. Presence and Biodistribution of Perfluorooctanoic Acid (PFOA) in Paracentrotus Lividus Highlight Its Potential Application for Environmental Biomonitoring. *Sci. Rep.* **2021**, *11*, 18763. [[CrossRef](#)]
89. Mashayekhi, V.; Tehrani, K.H.M.E.; Hashemzaei, M.; Tabrizian, K.; Shahraki, J.; Hosseini, M.-J. Mechanistic Approach for the Toxic Effects of Perfluorooctanoic Acid on Isolated Rat Liver and Brain Mitochondria. *Hum. Exp. Toxicol.* **2015**, *34*, 985–996. [[CrossRef](#)] [[PubMed](#)]
90. Steenland, K.; Fletcher, T.; Savitz, D.A. Epidemiologic Evidence on the Health Effects of Perfluorooctanoic Acid (PFOA). *Environ. Health Perspect.* **2010**, *118*, 1100–1108. [[CrossRef](#)] [[PubMed](#)]
91. Lindberg, C.D.; Di Giulio, R.T. Polycyclic Aromatic Hydrocarbon and Hypoxia Exposures Result in Mitochondrial Dysfunction in Zebrafish. *Aquat. Toxicol.* **2019**, *216*, 105298. [[CrossRef](#)] [[PubMed](#)]

- 
92. Müller, A.; Österlund, H.; Marsalek, J.; Viklander, M. The Pollution Conveyed by Urban Runoff: A Review of Sources. *Sci. Total Environ.* **2020**, *709*, 136125. [[CrossRef](#)]
  93. Khan, S.; Beigh, S.; Chaudhari, B.P.; Sharma, S.; Aliul Hasan Abdi, S.; Ahmad, S.; Ahmad, F.; Parvez, S.; Raisuddin, S. Mitochondrial Dysfunction Induced by Bisphenol A Is a Factor of Its Hepatotoxicity in Rats. *Environ. Toxicol* **2016**, *31*, 1922–1934. [[CrossRef](#)]
  94. Tener, R.F.; Holt, W.L. *Effect of Antioxidants on the Natural and the Accelerated Aging of Rubber*; National Bureau of Standards: Gaithersburg, MD, USA, 1935.
  95. Wong, H.-S.; Dighe, P.A.; Mezera, V.; Monternier, P.-A.; Brand, M.D. Production of Superoxide and Hydrogen Peroxide from Specific Mitochondrial Sites under Different Bioenergetic Conditions. *J. Biol. Chem.* **2017**, *292*, 16804–16809. [[CrossRef](#)]
  96. Joseph, A.M.; George, B.; Madhusoodanan, K.N.; Alex, R. Current Status of Sulphur Vulcanization and Devulcanization Chemistry: Process of Vulcanization. *Rubber Sci.* **2015**, *28*, 82–121.
  97. Brack, W.; Ait-Aissa, S.; Burgess, R.M.; Busch, W.; Creusot, N.; Di Paolo, C.; Escher, B.I.; Mark Hewitt, L.; Hilscherova, K.; Hollender, J.; et al. Effect-Directed Analysis Supporting Monitoring of Aquatic Environment—An in-Depth Overview. *Sci. Total Environ.* **2016**, *544*, 1073–1118. [[CrossRef](#)]